

# High-resolution radio observations of Seyfert galaxies in the extended 12-micron sample – II. The properties of compact radio components.

Andy Thean<sup>1,2</sup>, Alan Pedlar<sup>2</sup>, Marek J. Kukula<sup>3</sup>, Stefi A. Baum<sup>4</sup>  
and Christopher P. O’Dea<sup>4</sup>

<sup>1</sup> *Istituto di Radioastronomia del CNR, Via P. Gobetti 101, I-40129 Bologna, Italy*

<sup>2</sup> *Jodrell Bank Observatory, University of Manchester, Jodrell Bank, Macclesfield, Cheshire SK11 9DL, U.K.*

<sup>3</sup> *Institute for Astronomy, University of Edinburgh, Royal Observatory, Blackford Hill, Edinburgh EH9 3HJ*

<sup>4</sup> *Space Telescope Science Institute, 3700 San Martin Drive, Baltimore, Maryland 21218, USA*

1st Dec 2000

## ABSTRACT

We discuss the properties of compact nuclear radio components in Seyfert galaxies from the extended 12  $\mu\text{m}$  AGN sample of Rush et al. (1993). Our main results can be summarised as follows.

Type 1 and type 2 Seyferts produce compact radio components which are indistinguishable in strength and aspect, indicating that their central engines are alike as proposed by the unification model. Infrared *IRAS* fluxes are more closely correlated with low-resolution radio fluxes than high-resolution radio fluxes, suggesting that they are dominated by kiloparsec-scale, extra-nuclear emission regions; extra-nuclear emission may be stronger in type 2 Seyferts. Early-type Seyfert galaxies tend to have stronger nuclear radio emission than late-type Seyfert galaxies. V-shaped extended emission-line regions, indicative of ‘ionisation cones’, are usually found in sources with large, collimated radio outflows. Hidden broad lines are most likely to be found in sources with powerful nuclear radio sources. Type 1 and type 2 Seyferts selected by their *IRAS* 12  $\mu\text{m}$  flux densities have well matched properties.

## Key words:

galaxies: active – galaxies: Seyfert – galaxies: statistics – infrared: galaxies – radio continuum: galaxies.

## 1 INTRODUCTION

Much of the progress in understanding the physics of active galaxies has been made by studying the sub-class known as Seyfert galaxies. Seyfert galaxies are more common, in terms of their space density, than radio galaxies or quasars, and nearby examples can be identified and studied in detail. Their nuclei are bright enough to be observed in most regions of the electromagnetic spectrum using various techniques and their stellar populations can be studied more easily than those of more distant classes of active galaxy. The wide variety of good quality survey information available about Seyfert galaxies means that valuable insights into their behaviour can be obtained using statistical techniques i.e. samples of Seyfert galaxies can be selected using a choice of parameters and used to address a range of open questions. In this paper we investigate the properties of the compact radio components found at Seyfert nuclei by using one of the

largest homogeneously-selected samples of Seyfert galaxies available.

The central engines of Active Galactic Nuclei (AGN) are thought to contain supermassive black holes surrounded by energy-emitting accretion discs. Unique information about Seyfert central engines can be obtained from high-resolution radio observations. The strengths of the radio cores show the level of nuclear activity, even in dust-enshrouded sources, and may indicate the masses of the supermassive black holes (Franceschini, Vercellone & Fabian 1998). In addition, small-scale, collimated radio structures reveal outflows which are thought to dominate the structure and dynamics of Seyfert narrow-line regions (Falcke, Wilson & Simpson 1998; Axon et al. 1998; Capetti et al. 1999) and probably indicate the position angles of the central accretion discs.

Despite the influence of radio outflows on the narrow-line region, at present they do not play an important rôle in Seyfert unification models. According to these models

arXiv:astro-ph/0103266v1 16 Mar 2001

there is one population of intrinsically similar objects whose orientation determines their observed properties. It is proposed that the sub–parsec–scale broad–line–emitting region in type 2 sources is hidden by a suitably oriented dusty torus and only narrow emission lines from the larger narrow–line–emitting region are seen; in type 1 sources the orientation of the torus allows both broad and narrow lines to be observed (see Antonucci 1993).

Recent radio surveys indicate that the radio properties of type 1 and type 2 Seyferts are generally well matched, in support of the unification model (Edelson 1987; Ulvestad & Wilson 1989; Giuricin et al. 1990; Kukula et al. 1995; Rush, Malkan & Edelson 1996; Nagar et al. 1999; Morganti et al. 1999). Early radio surveys which found differences between type 1 and type 2 Seyferts (Ulvestad & Wilson 1984a; Ulvestad & Wilson 1984b) were probably affected by selection effects (Salzer 1989; Wilson 1991), but there remain a handful of recent results which are not readily explained by the unification model e.g. Roy et al. (1994) found that the detection rate of compact radio cores smaller than 0.1 arcsec was significantly lower for type 1 Seyferts than for type 2 Seyferts, and observations by Kukula et al. (1995) show that an excessively high fraction of type 1 Seyferts are unresolved at 0.25 arcsec resolution.

This paper is organised as follows; in Section 2 we describe the sample, the data and the statistical tests used in our analysis, in Section 3 we compare the compact nuclear radio components found in type 1 and type 2 Seyfert galaxies, in Section 4 we discuss the origin of the *IRAS* emission from Seyfert galaxies, in Section 5 we examine the relationship between host galaxy and the central engine, in Section 6 we examine the radio properties of Seyferts with V–shaped extended emission line regions, in Section 7 we examine the radio properties of Seyferts with known hidden broad–line regions, in Section 8 we discuss the sample selection and in Section 9 we give a summary of our results.

A value of  $H_0 = 75 \text{ km s}^{-1} \text{ Mpc}^{-1}$  is assumed throughout.

## 2 SAMPLE, DATA AND STATISTICAL TESTS

Our results are based on radio observations of the extended 12  $\mu\text{m}$  sample of Rush, Malkan & Spinoglio (1993) made with the VLA in A–configuration at 8.4 GHz (Thean et al. 2000a). These 0.25–arcsec–resolution observations allow elongated radio structures tens of parsecs in size to be resolved and enable radio components smaller than 3.5 arcsec to be isolated from kiloparsec–scale, low–brightness–temperature emission (see Thean et al. 2000b for a discussion of instrumental limitations). The typical 1– $\sigma$  noise level was 50  $\mu\text{Jy}/\text{beam}$ . In addition to our new observations we make use of archive data from the *IRAS* survey as obtained from Rush, Malkan & Spinoglio (1993), the 1.4 GHz NRAO VLA Sky Survey (NVSS) described by Condon et al. (1998), the Lyon–Meudon Extragalactic Database (LEDA) described by Paturel et al. (1996) and the NASA/IPAC Extragalactic Database (NED) described by Helou et al. (1995). All archive data used in our analysis are given in Appendix A.

The extended 12  $\mu\text{m}$  AGN sample is an extension of the original 12  $\mu\text{m}$  AGN sample of Spinoglio & Malkan (1989)

to fainter flux levels using the *IRAS Faint Source Catalogue Version 2* (Moshir 1991). From an initial sample of 893 mid–infrared–bright sources, AGN catalogues were used to define a sub–sample of active galaxies which contains 118 objects, the majority of which are Seyfert galaxies. The sample is one of the largest homogeneously–selected samples of Seyferts available and appears to contain representative populations of galaxies with type 1 and type 2 optical spectra; Spinoglio & Malkan (1989) proposed that the *IRAS* 12  $\mu\text{m}$  waveband carries an approximately constant fraction, around 20%, of the bolometric flux for quasars and both types of Seyfert (selection effects are discussed in Section 8). In order to restrict our analysis to well–identified Seyfert galaxies, we have excluded 11 sources from our analysis of the extended 12  $\mu\text{m}$  AGN sample and reclassified two. The exclusion of two LINERs (NGC 1097 and NGC 3031) and 3 starburst galaxies (NGC 1386, Arp 220 and NGC 6810) and the reclassification of two Seyfert 1s as Seyfert 2s (Markarian 6 and NGC 2992) follows Dopita et al. (1998), the exclusion of one starburst galaxy (NGC 34) follows Mulchaey, Wilson & Tsvetanov (1996a) and the exclusion of five radio–loud sources (3C 120, 3C 234, 3C 273, 3C 445 and OJ 287) follows Paper I (Thean et al. 2000a). The resulting sample contains 47 type 1 Seyferts and 60 type 2 Seyferts. As pointed out by Hunt & Malkan (1999), the accurate spectroscopic classification of the sample is still not complete. In Section 8.3 we identify 38 sources which are classified as normal or high–far–infrared galaxies by Rush, Malkan & Spinoglio (1993), but which are classified as Seyfert galaxies in the NED.

Our analysis has been carried out using univariate two–sample tests and bivariate correlation tests based on Survival Analysis techniques, which allow information about censored data (size and flux density upper–limits) to be used efficiently. Tests based on Survival Analysis were implemented using the software ASURV (Lavalley, Isobe & Feigelson 1992). Two–sample tests available with ASURV have been discussed by Feigelson & Nelson (1985) and include two versions of the Gehan’s test (permutation variance and hypergeometric variance), the Logrank test, the Peto & Peto test and the Peto & Prentice test. Correlation tests have been discussed by Isobe, Feigelson & Nelson (1986) and include the Cox Proportional Hazard test, Kendall’s Tau and Spearman’s Rho. For ease of comparison, we have maintained the use of these tests even when no censored data have been used, in these cases the Peto & Prentice test reduces to the Gehan’s test and we are able to apply the Kolmogorov–Smirnov (KS) test. We have used these tests to determine the probability of obtaining a test statistic under a given null hypothesis; usually the null hypothesis states that two distributions are drawn at random from the same parent population for two–sample tests, or that there is no correlation between two variables for correlation tests. We adopt the convention that a result is *marginally significant* if the probability of the null hypothesis,  $P(\text{null})$ , is less than 5% for at least one test, *significant* if  $P(\text{null})$  is less than 5% for all tests, *highly significant* if  $P(\text{null})$  is less than 1% for all tests and *extremely significant* if  $P(\text{null})$  is less than 0.1% for all tests. Where censored data has been used, cumulative distributions are plotted using the Kaplan–Meier estimator which is a non–parametric, maximum–likelihood estimator of a randomly–censored sample (see Feigelson & Nelson 1985). For each plot we display the mean uncertainty

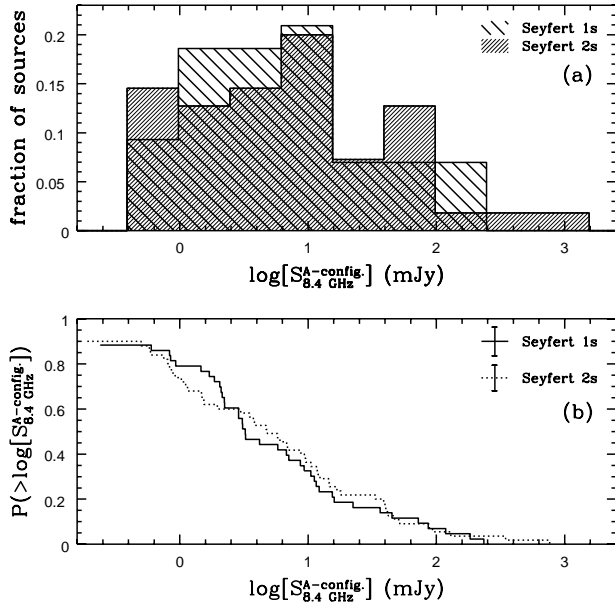


**Figure 1.** (a) Histograms showing the fractional 8.4 GHz A-configuration flux density distributions of the 38 type 1 and 48 type 2 Seyferts from the extended 12  $\mu\text{m}$  sample which were detected. (b) The cumulative flux density distributions of the 43 type 1 and 55 type 2 Seyferts observed, as given by the Kaplan–Meier estimator where the y axis gives the probability that a source is brighter than a given flux density. The flux density distributions of the two Seyfert types are statistically indistinguishable.

of all points on the cumulative distribution as calculated using ASURV.

### 3 COMPACT RADIO COMPONENTS IN TYPE 1 AND TYPE 2 SEYFERTS

#### 3.1 The strength of the radio emission

Figure 1 shows the 8.4 GHz A-configuration flux density distributions of type 1 and type 2 Seyferts from the extended 12  $\mu\text{m}$  sample. There is no significant difference between the 8.4 GHz A-configuration flux densities of type 1 and type 2 Seyferts. The probability of the null hypothesis, that the two flux density distributions are drawn at random from the same parent population, is: 89.98% (Gehan’s, perm.), 90.02% (Gehan’s, hyper.), 92.95% (Logrank test), 91.21% (Peto & Peto) and 91.19% (Peto & Prentice).

Figures 2(a) and 2(b) show the 8.4 GHz A-configuration luminosity distributions of type 1 and type 2 Seyferts from the sample. The two distributions are statistically indistinguishable, and span approximately the same range in luminosity, from  $1 \times 10^{18.6}$  to  $1 \times 10^{24.0}$   $\text{WHz}^{-1}$ . The probability of the null hypothesis, that the two luminosity distributions are drawn at random from the same parent population, is: 70.86% (Gehan’s, perm.), 70.87% (Gehan’s, hyper.), 77.76% (Logrank test), 71.22% (Peto & Peto) and 71.48% (Peto & Prentice). In order to estimate the magnitude of the systematic difference in luminosity which would allow the null hypothesis to be rejected we have made trials with the ob-

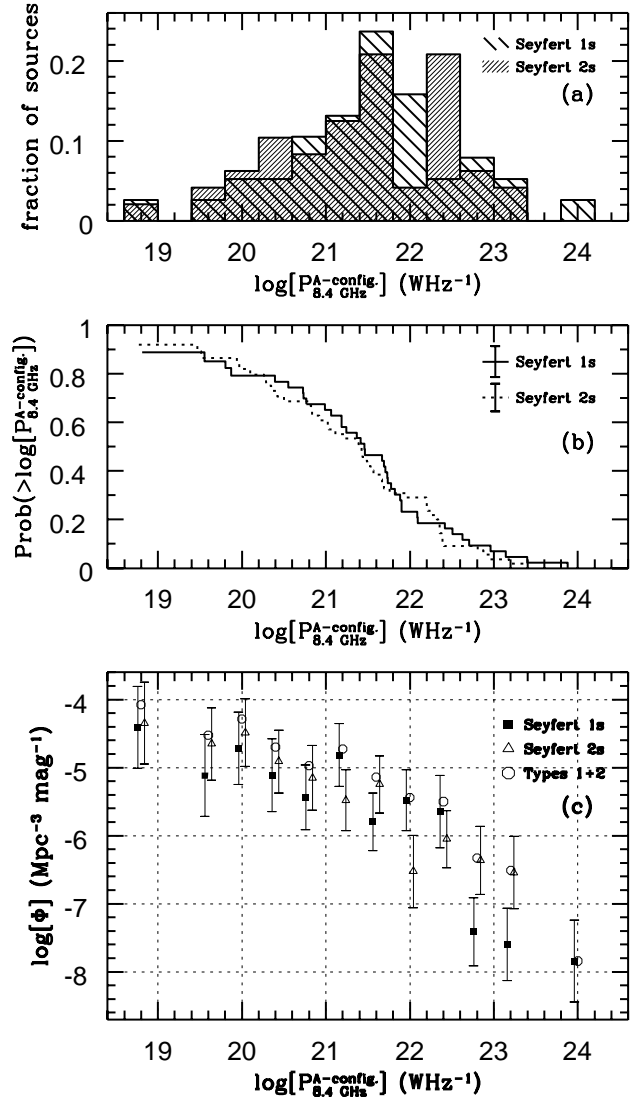


**Figure 2.** (a) The fractional 8.4 GHz A-configuration luminosity distributions of the 38 type 1 and 48 type 2 Seyferts from the extended 12  $\mu\text{m}$  sample which were detected. (b) The cumulative 8.4 GHz A-configuration luminosity distributions of the 43 type 1 and 55 type 2 Seyferts observed, as given by the Kaplan–Meier estimator. The luminosity distributions of the two Seyfert types are indistinguishable and this suggests that they contain the same type of central engine. (c) The absolute space densities of the two Seyfert types have been estimated by normalising the differential 8.4 GHz VLA A-configuration radio luminosity functions. For display purposes, points representing the bin centres of Seyfert type 2s and Seyfert types 1 and 2, have been offset by values of  $\log(P) = -0.04$  and  $\log(P) = 0.04$  respectively.

servational data. By scaling the luminosity of the Seyfert 1 sub-population and repeating the two-sample tests, we find that the probability of the null hypothesis is less than 5% for all statistical tests when scaling factors less than or equal to one sixth or greater than or equal to four are applied (see Appendix B for test results using various scaling factors).

Figure 2(c) shows the differential 8.4 GHz A-configuration luminosity function of the extended 12  $\mu\text{m}$  Seyfert sample (the construction of the differential luminos-

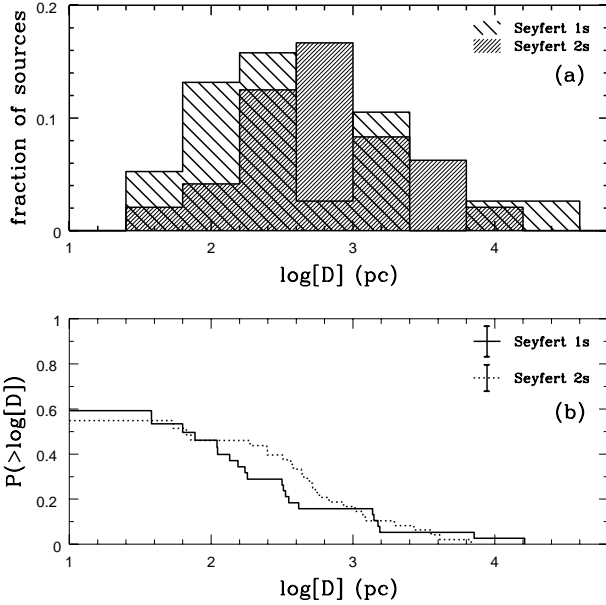


**Figure 3.** (a) The fractional size distributions of the 20 type 1 and 25 type 2 Seyferts from the extended  $12\ \mu\text{m}$  sample which were resolved. (b) The cumulative size distributions of the 38 type 1 and 48 type 2 Seyferts detected, as given by the Kaplan–Meier estimator where the y axis gives the probability that a source is larger than a given size. The two size distributions are statistically indistinguishable indicating that type 1 and type 2 Seyferts have an equal capacity for producing extended nuclear radio components.

ity function is described in Appendix C). According to the unification model, the relative space densities of Seyfert 1s and Seyfert 2s are determined by the typical opening angle of the circum–nuclear torus. We have used 3 methods to estimate a typical opening angle from the differential radio luminosity function, all methods give a type 1 to type 2 ratio less than unity, but this quantity is poorly constrained. Summing  $\Phi(L)$  over bins containing both Seyfert type 1s and Seyfert type 2s yields a cone opening angle of  $110_{-50}^{+20}$  degrees (using all such bins) and  $150_{-50}^{+10}$  degrees (using only those 3 bins containing more than 4 sources); errors are calculated by taking the uncertainty in  $\Phi(L)$  values as proportional to the Poisson noise in each bin. Integrating linear power law fits over the observed range in radio power ( $1 \times 10^{18.4}$  to  $1 \times 10^{24.0}\ \text{WHz}^{-1}$ ) yields an opening angle of  $60_{-10}^{+10}$  degrees, but because the type 1 and type 2 fits have different gradients this value is sensitive to the lower radio power limit used (fits were sought only for luminosity bins containing more than 4 sources and the uncertainty in the opening angle is derived from the uncertainty in the fits).

### 3.2 Radio source sizes

Table 1 shows the number of sources of each structural type within the full sample and within a sub–sample of sources with 8.4 GHz flux densities greater than 5 mJy/beam (typically  $100\text{--}\sigma$ ). Structural types,  $T_{\text{rad}}$ , follow the notation used by Ulvestad & Wilson (1984a): U for single unresolved sources, S for single slightly–resolved sources, A for sources

Radio components	$T_{\text{rad}}$	Full sample		$S_{8.4} > 5\ \text{mJy}$	
		Type 1	Type 2	Type 1	Type 2
1 unresolved	U	19 (40%)	22 (37%)	6 (32%)	8 (30%)
1 slightly–resolved	S	9 (19%)	6 (10%)	7 (37%)	4 (15%)
2	L	3 (6%)	6 (10%)	0 (0%)	4 (15%)
>2 linearly–aligned	L	4 (9%)	7 (12%)	3 (16%)	6 (22%)
Diffuse	D	0 (0%)	2 (3%)	0 (0%)	2 (7%)
Diffuse + unresolved	D+U	0 (0%)	1 (2%)	0 (0%)	1 (4%)
Ambiguous	A	3 (6%)	3 (5%)	3 (16%)	2 (7%)
unobserved	-	4 (9%)	5 (8%)	-	-
undetected	-	5 (11%)	8 (13%)	-	-
Total		47	60	19	27

**Table 1.** The 8.4 GHz A–configuration radio structures of Seyferts from the extended  $12\ \mu\text{m}$  sample. The true distribution of radio morphologies is more accurately represented by a sub–sample of sources brighter than 5 mJy/beam for which high–dynamic–range maps are available.

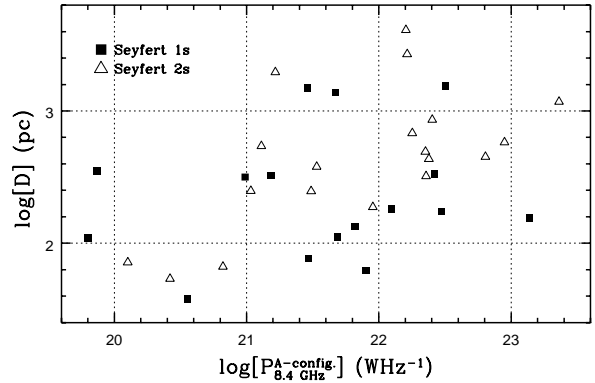


**Figure 4.** Radio size is plotted against radio power for collimated sources (types S and L) from the extended  $12\ \mu\text{m}$  Seyfert sample. There is a statistically significant correlation between radio power and radio size for type 2 Seyferts, but not for type 1 Seyferts.

with ambiguous structures, D for sources with diffuse structures and L for sources with possible linear structures.

Figure 3 shows the size distributions of the nuclear radio structures in type 1 and type 2 Seyferts from the extended  $12\ \mu\text{m}$  sample. Each Seyfert type shows an approximately equal fraction of unresolved sources (around half) and the two size distributions are statistically indistinguishable. The probability of the null hypothesis, that type 1 and type 2 size distributions are drawn at random from the same parent population, is: 53.00% (Gehan’s, perm.), 53.16% (Gehan’s, hyper.), 78.93% (Logrank), 59.69% (Peto & Peto) and 59.51% (Peto & Prentice). To estimate the magnitude of the systematic difference in sizes which would allow the null hypothesis to be rejected we have made trials with the observational data. By scaling the sizes of the Seyfert 1 sub–population and repeating the two–sample tests, we find that the probability of the null hypothesis is less than 5% for all statistical tests when scaling factors less than or equal to one sixth and greater than or equal to 10 are applied (see Appendix B for test results using various scaling factors).

Figure 4 shows how radio size varies with radio power for sources which have slightly–resolved, double or linearly–aligned radio components (structural types S or L). There

is a statistically significant correlation between radio size and radio power for this sub-population. The probability of the null hypothesis, that there is no correlation between radio size and radio power, is: 2.19% (Cox proportional Hazard), 1.91% (Kendall's Tau) and 1.37% (Spearman's Rho). Interestingly, the correlation is only significant for type 2 sources. For the 16 type 1 sources the probability of the null hypothesis is: 50.43% (Cox proportional Hazard), 52.85% (Kendall's Tau) and 56.90% (Spearman's Rho). For the 19 type 2 sources the probability of the null hypothesis is: 3.04% (Cox proportional Hazard), 1.91% (Kendall's Tau) and 2.02% (Spearman's Rho).

For the extended 12  $\mu\text{m}$  Seyfert sample as a whole, sources with type S or type L radio sources have higher radio luminosities than Seyferts of other structural types, but this result may be partly attributable to the difficulty in detecting collimated structures in faint sources; resolved sources can be wrongly classified as unresolved if their secondary flux components fall below the flux limit. For the Seyfert sample as a whole, the probability of the null hypothesis, that sources with type S or type L radio structures and sources with other types of radio structure have luminosity distributions which are drawn at random from the same parent population, is: 0.18% (Gehan's, perm.), 0.11% (Gehan's, hyper.), 0.02% (Logrank), 0.16% (Peto & Peto) and 0.18% (Peto & Prentice). However, for a bright sub-population of 46 sources with 8.4 GHz A-configuration flux densities higher than 5 mJy/beam there is no significant difference between the radio luminosities of sources with type S or type L radio structures and sources with other structural types, the probability of the null hypothesis is: 45.47% (Gehan's, perm.), 45.34% (Gehan's, hyper.), 96.39% (Logrank) and 96.39% (Peto & Peto).

Note that some of the most luminous sources in the sample are unresolved at our resolution. This sub-population of bright, unresolved sources includes two of the three most luminous radio sources in the sample (Markarian 231 and Markarian 348) and the three most 'radio-loud' Seyferts in the sample (Markarian 348, F01475-0704 and NGC 7213 have the highest 8.4 GHz A-configuration to *IRAS* 60  $\mu\text{m}$  flux ratios).

### 3.3 Implications: the central engines of type 1 and type 2 sources are alike.

Our results, which are based on the largest sub-arcsecond-resolution radio imaging survey of a homogeneously-selected sample of Seyfert galaxies available, provide the most stringent comparison of the radio powers and radio sizes of Seyfert nuclei to date. The fact that we find no significant differences between the strengths, sizes and morphologies of compact radio components in type 1 and type 2 Seyfert galaxies is evidence that their central engines are alike, as proposed by unification models.

According to the unification model, obscuration by a circum-nuclear dusty tori gives rise to the differences between the observational properties of type 1 and type 2 Seyferts, but, since dust is transparent at radio wavelengths, their radio luminosities are expected to be equivalent. In agreement with previous high-resolution surveys (Kukula et al. 1995; Nagar et al. 1999), we have found that the 8.4 GHz A-configuration radio luminosities of the two Seyfert

types are statistically indistinguishable (§3.1) and we estimate that if systematic differences in luminosity are present they are less than a factor of six. We find no evidence of orientation-dependent free-free absorption, but our luminosity comparison is not very sensitive to such effects because we have included extra-nuclear flux components and because free-free absorption is not expected to be strong at 8.4 GHz (e.g. Krolik & Lepp 1989).

The fact that the radio structures of type 1 and type 2 Seyferts are statistically indistinguishable (§3.2) is also consistent with the Seyfert unification model. According to the unification model, the two Seyfert types have an equal capacity for producing collimated radio structures and differ only by their orientation. Orientation is expected to make the observed radio structures in Seyfert type 2s systematically larger than those in Seyfert type 1s (if the axis of the obscuring torus is aligned with the radio collimation axis, type 1 Seyferts should be geometrically fore-shortened), but variations in intrinsic source length are expected to dominate the effects of orientation, especially for models of tori with intermediate opening angles. We estimate that our tests are only able to reject the hypothesis that the sizes of the two Seyfert types are equivalent for systematic differences in size greater than an approximate factor of 8 and therefore they are probably insensitive to the effects of orientation. The statistically insignificant trend for the radio sources in type 2 Seyferts to be larger than those in Seyfert 1s (Fig. 3) and the relative fractions of sources with type S and type L radio structures in a bright sub-sample (Table 1) are in the sense predicted by the unification model.

Observations of the Early-type Seyfert sample (Nagar et al. 1999), and the CfA Seyfert sample (Kukula et al. 1995) have shown that type 1 Seyferts are more likely to have unresolved nuclear radio structures than type 2 Seyferts. For the CfA Seyfert sample and a volume-limited southern Seyfert sample (Morganti et al. 1999) the difference between the size distributions of type 1 and type 2 Seyferts is statistically significant (this is not the case for the Early-type Seyfert sample). VLA A-configuration observations of the CfA sample at 8.4 GHz show that only one type 1 Seyfert is fully resolved compared to nine type 2 Seyferts. The probability that the radio size distributions of type 1 and type 2 CfA Seyferts are drawn at random from the same parent population is: 0.59% (Gehan's, perm.), 0.53% (Gehan's, hyper.), 1.28% (Logrank), 0.84% (Peto & Peto) and 0.78% (Peto & Prentice). Note however, that the difference in size between type 1 and type 2 Seyferts in the CfA sample may be related to a bias against distant type 2 Seyferts (see §8.1); whether a similar bias affects the southern Seyfert sample of Morganti et al. is unclear. A bias against distant type 2 Seyferts can affect observed size distributions because a resolved radio source is more likely to appear unresolved if it is more distant; for most sources, this is because secondary flux components fall below the flux limit rather than the effect of fixed angular resolution. If the redshifts of all type 2 Seyferts in the CfA sample are scaled by a factor of 1.6 (the average difference between the type 2 and type 1 redshifts, as estimated from linear fits to the cumulative redshift distributions), three previously resolved sources become unresolved and the size difference between type 1 and type 2 Seyferts is no longer statistically significant.

The only difference we have found between the com-

pact radio components in type 1 and type 2 Seyferts is that the latter show a significant correlation between radio size and radio power whereas the former do not. Weaker evidence of this difference has been found previously (Nagar et al. 1999). The difference is in the sense predicted by the Seyfert unification model, according to which a correlation between radio size and radio power should be clearest for type 2 Seyferts; the observed angular sizes of elongated sources whose axes are close to the line of sight are less reliable indicators of true source sizes than the angular sizes of sources lying close to the plane of the sky i.e. it is possible that large type 1 sources can project small apparent sizes whereas large type 2 sources cannot. According to the unification model, the radio sizes of type 1 Seyferts should show a looser, flatter dependence on radio power than those of type 2 Seyferts. Our data are broadly consistent with such predictions, but more data is required to test them. The correlation between radio size and radio power for type 2 Seyferts confirms the results of previous studies (Ulvestad & Wilson 1984b; Giuricin et al. 1990; Nagar et al. 1999; Morganti et al. 1999).

The size of an expanding outflow is a primary indicator of its age and therefore one interpretation of the matched size distributions of type 1 and type 2 Seyferts is that they evolve similarly and have similar ages. Recent HST spectroscopy has been used to provide an upper-limit of  $1.5 \times 10^5$  years on the age of the kiloparsec radio outflow in Markarian 3 (Capetti et al. 1999). Our results confirm that compact nuclear outflows on this scale are rare, and suggest that around 80% to 90% of Seyfert nuclear outflows are younger than that of Markarian 3. Compact nuclear outflows appear to be small or absent in a considerable fraction of sources; approximately 30% of sources for which high-dynamic-range maps are available are unresolved (smaller than around 100 parsecs). This fraction is too high to be explained by models in which all Seyferts produce radio outflows which advance at the speed of the largest sources and probably reflects a combination of factors such as instrumental limitations, the fraction of Seyferts capable producing radio outflows, duty cycle patterns and outflow evolution. Note that our observations are insensitive to low-brightness-temperature flux components and therefore source sizes have been under-estimated in cases where the nucleus produces extended, diffuse emission.

We can be confident that those sources with the youngest radio outflows are to be found in the sub-population of unresolved sources. Possible examples of young outflows are provided by Markarian 231 and Markarian 348, which share some of the properties of Compact Symmetric Objects (CSOs) and Gigahertz Peaked Spectra (GPS) galaxies (Ulvestad et al. 1999) which are probably young radio-loud AGN. If the compact radio sources in Markarian 231 and Markarian 348 are indeed caused by young nuclear outflows, the fact that they are more powerful than the largest sources in the sample implies that radio outflows are particularly luminous in their early stages; similar suggestions have been made to explain the properties of the CSO/GPS population (see O’Dea 1998). Furthermore we may speculate that if they are to fit the correlation between radio size and radio power shown in Figure 4, Markarian 231 and Markarian 348 will decrease in luminosity rapidly (a few orders of magnitude before reaching scales of hun-

dreds of parsecs) and if the correlation between size and power represents an evolutionary sequence, their luminosities will increase again in later stages of evolution. Note that both Markarian 231 and Markarian 348 show diffuse radio emission tens of kiloparsecs in extent, but whether such diffuse outflows are caused by previous AGN activity or starburst-driven superwinds is unclear (Baum et al. 1993; Colbert et al. 1996; Colbert et al. 1998).

Finally, we note that Franceschini, Vercellone & Fabian (1998) have shown a correlation between the 5 GHz radio power of a galactic nucleus and the dynamical mass of its central black hole. If this result can be generalised, our results imply that the masses of the black holes in type 1 and type 2 Seyferts are equivalent. Given the steep dependence of radio power on black hole mass claimed by Franceschini, Vercellone & Fabian (1998), the radio luminosities we have observed imply a range of black hole masses spanning only 2 orders of magnitude (around  $10^{7.5}$  to  $10^{9.5} M_{\odot}$  for a radio spectral index of  $-0.7$ ).

## 4 THE ORIGIN OF IRAS EMISSION FROM SEYFERT GALAXIES

### 4.1 High-resolution radio fluxes

In Figure 5 the 8.4 GHz A-configuration flux densities of Seyferts from the extended 12  $\mu\text{m}$  sample are plotted against their *IRAS* flux densities. The probability of the null hypothesis, that there is no correlation between 8.4 GHz A-configuration fluxes and *IRAS* fluxes for each *IRAS* waveband, is given in Table 2. The only significant correlation between 8.4 GHz A-configuration fluxes and *IRAS* fluxes is found at 25  $\mu\text{m}$ ; there are marginally significant correlations at 12  $\mu\text{m}$  and 60  $\mu\text{m}$ , but no evidence of a correlation at 100  $\mu\text{m}$ . In most cases, the 8.4 GHz A-configuration flux densities of Seyferts with a given *IRAS* flux density vary by at least two orders of magnitude.

In Figure 6 we plot 8.4 GHz A-configuration luminosities against *IRAS* 12  $\mu\text{m}$  luminosities. For a flux-limited sample, correlations between luminosities in different wavebands can be misleading because of the strong dependence of luminosity on distance. In fact, the 8.4 GHz versus 12  $\mu\text{m}$  luminosity-luminosity plane is evenly filled between the limits defined by the Malmquist bias and the flux limits (see Appendix D) and evidence of a true correlation is weak. Some evidence of a real (steep) dependence of 8.4 GHz A-configuration luminosity on *IRAS* 12  $\mu\text{m}$  luminosity is given by the distribution of radio flux density upper-limits, but this dependence should be judged using partial correlation methods (Akritas & Siebert 1996) when the effects of sample incompleteness are properly understood; the extended 12  $\mu\text{m}$  sample was selected using an *IRAS* flux limit of 0.22 Jy, but it is only complete to 0.3 Jy (Rush, Malkan & Spinoglio 1993).

### 4.2 Low-resolution radio fluxes

Figure 7 shows how integrated VLA NVSS radio flux densities vary with *IRAS* flux densities for the extended 12  $\mu\text{m}$  Seyfert sample. The probability that NVSS fluxes and *IRAS* fluxes are correlated is extremely significant for each

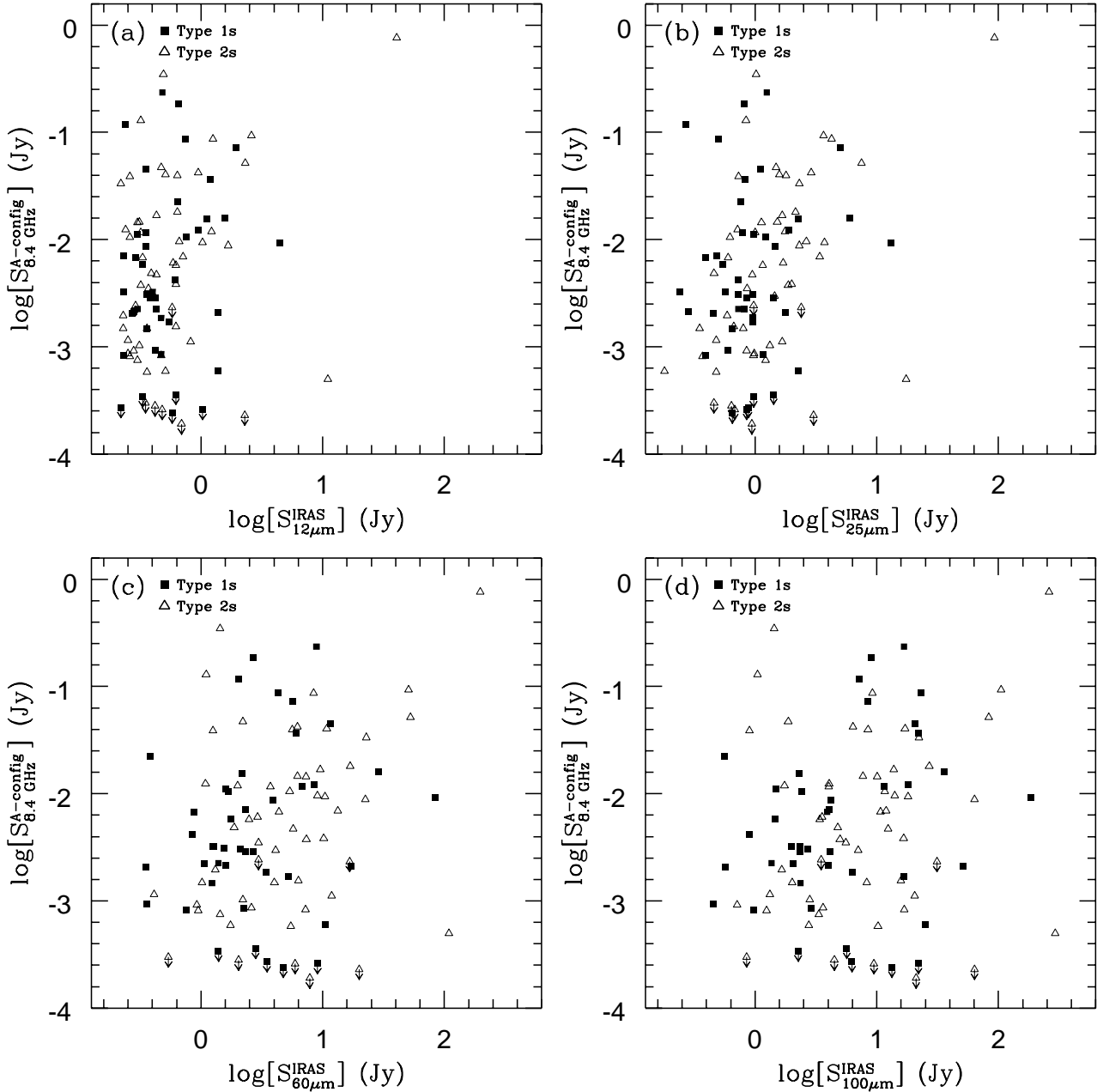


**Figure 5.** VLA 8.4 GHz A-configuration radio flux densities are plotted against (a) 12  $\mu\text{m}$ , (b) 25  $\mu\text{m}$ , (c) 60  $\mu\text{m}$  and (d) 100  $\mu\text{m}$  *IRAS* flux densities for Seyferts from the extended 12  $\mu\text{m}$  sample. The only significant correlation between 8.4 GHz A-configuration fluxes and *IRAS* fluxes is found at 25  $\mu\text{m}$ ; there are marginally significant correlations at 12  $\mu\text{m}$  and 60  $\mu\text{m}$ , but no evidence of a correlation at 100  $\mu\text{m}$ . Radio flux density upper-limits are denoted by arrows.

*IRAS* waveband. Interestingly, correlations between NVSS fluxes and *IRAS* fluxes are stronger for all *IRAS* wavebands when integrated NVSS fluxes are used instead of peak NVSS fluxes. Table 2 gives individual test results.

Figure 8 shows how peak NVSS flux densities vary with 8.4 GHz A-configuration flux densities. The two variables are likely to be correlated; the probability of the null hypothesis, that there is no correlation between the 8.4 GHz fluxes (independent variable) and the NVSS peak fluxes, is: 0.50% (Cox proportional Hazard), 1.37% (Kendall's Tau)

and 2.12% (Spearman's Rho). For 8.4 GHz fluxes and NVSS integrated fluxes the probability of the null hypothesis is: 0.56% (Cox proportional Hazard), 1.61% (Kendall's Tau) and 2.41% (Spearman's Rho).

The apparent spectral index estimated by comparing 8.4 GHz A-configuration flux densities and NVSS peak flux densities may be regarded as a lower limit on the spectral index of the active nucleus since NVSS fluxes contain a higher fraction of non-nuclear emission than A-configuration fluxes. The apparent spectral indices measured

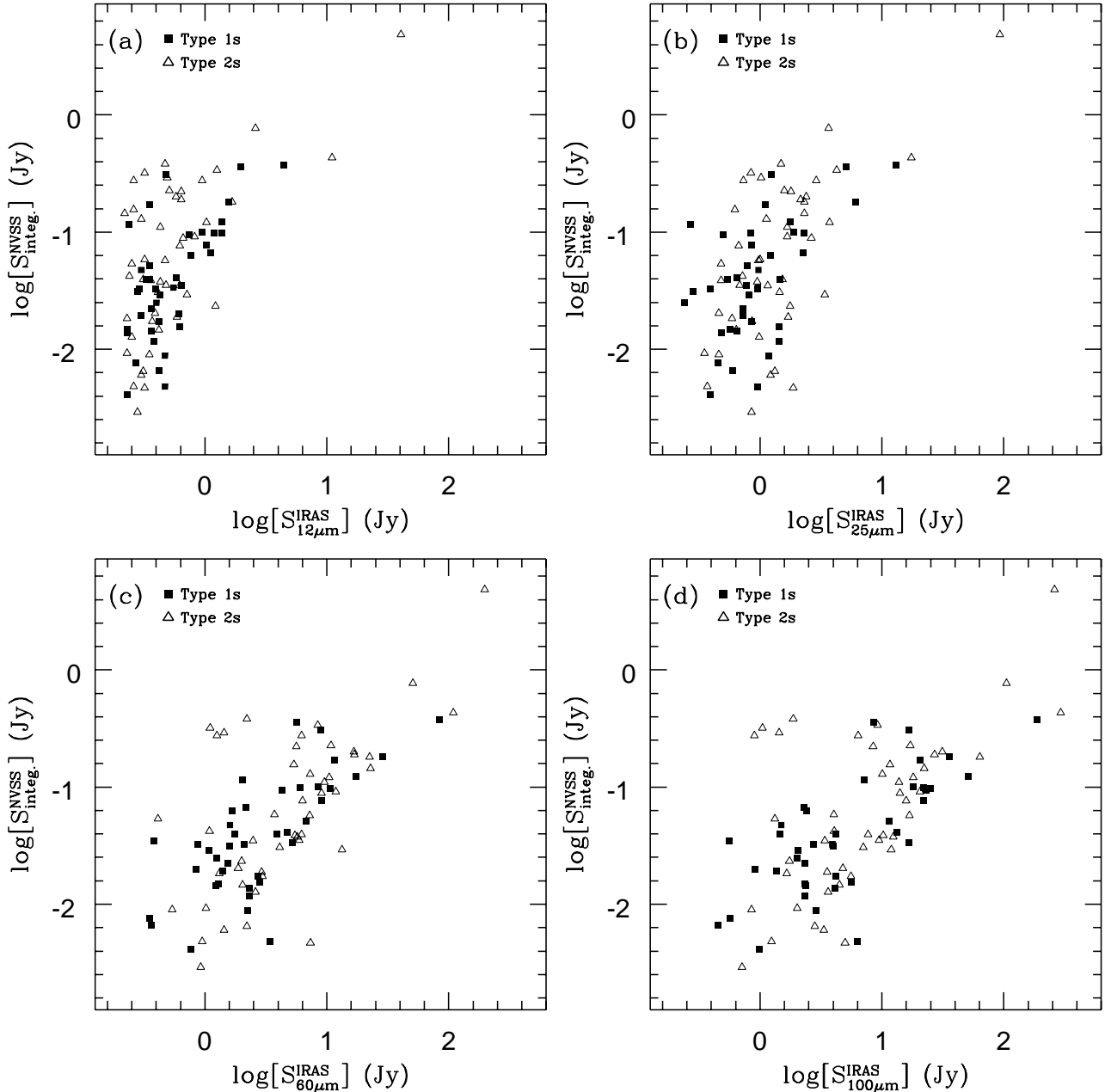


**Figure 7.** Integrated NVSS radio flux densities are plotted against (a) 12  $\mu\text{m}$ , (b) 25  $\mu\text{m}$ , (c) 60  $\mu\text{m}$  and (d) 100  $\mu\text{m}$  *IRAS* flux densities. There are extremely significant correlations between NVSS fluxes and infrared fluxes in each *IRAS* waveband. The group of four type 2 Seyferts centered near  $\log[S_{100\mu\text{m}}^{\text{IRAS}}]=0.1$  and  $\log[S_{\text{integ.}}^{\text{NVSS}}]=-0.5$  in (d) contains three sources with known hidden broad lines (F01475–0740, Markarian 348 and Markarian 463) and one which has been classified as both type 1 and type 2 (Markarian 6).

in this way lie in the range  $-1.4 < \alpha < 0$  for 80% of the sources.

### 4.3 Implications: *IRAS* fluxes are dominated by large-scale emission.

The correlations between 8.4 GHz A-configuration fluxes and the fluxes in all *IRAS* wavebands (§4.1) are much weaker than the corresponding relationships between NVSS fluxes and *IRAS* fluxes (§4.2). This result indicates that large-

scale extra-nuclear emission dominates *IRAS* fluxes for the Seyferts in the sample.

It is difficult to explain the differences between the radio to infrared correlations obtained with 1.4 GHz NVSS fluxes and 8.4 GHz A-configuration fluxes solely in terms of differences in frequency, and the differences between the radio to infrared correlations obtained with NVSS peak fluxes and NVSS integrated fluxes (§4.2) can only be due to the effect of spatially distinct flux components; the fact that correlations between NVSS fluxes and fluxes at all *IRAS*



Independent variable	Dependent variable	Cox		Kendall's $\tau$		Spearman's $\rho$	
		P(null)	$\chi^2$	P(null)	Z	P(null)	$\rho$
S <sub>12<math>\mu</math>m</sub> IRAS	S <sub>8.4GHz</sub> A-con.	33.18%	0.942	4.26%	2.028	5.62%	0.194
S <sub>25<math>\mu</math>m</sub> IRAS	S <sub>8.4GHz</sub> A-con.	1.47%	5.947	0.14%	3.203	0.21%	0.313
S <sub>60<math>\mu</math>m</sub> IRAS	S <sub>8.4GHz</sub> A-con.	20.85%	1.582	2.72%	2.209	3.97%	0.209
S <sub>100<math>\mu</math>m</sub> IRAS	S <sub>8.4GHz</sub> A-con.	64.90%	0.207	9.09%	1.691	13.76%	0.151
S <sub>12<math>\mu</math>m</sub> IRAS	S <sub>peak</sub> NVSS	0.00%	16.530	0.01%	3.922	0.02%	0.393
S <sub>25<math>\mu</math>m</sub> IRAS	S <sub>peak</sub> NVSS	0.00%	21.074	0.00%	4.764	0.00%	0.470
S <sub>60<math>\mu</math>m</sub> IRAS	S <sub>peak</sub> NVSS	0.00%	17.404	0.00%	4.875	0.00%	0.480
S <sub>100<math>\mu</math>m</sub> IRAS	S <sub>peak</sub> NVSS	0.05%	12.044	0.00%	4.250	0.01%	0.423
S <sub>12<math>\mu</math>m</sub> IRAS	S <sub>integ</sub> NVSS	0.00%	25.471	0.00%	4.782	0.00%	0.466
S <sub>25<math>\mu</math>m</sub> IRAS	S <sub>integ</sub> NVSS	0.00%	23.794	0.00%	5.044	0.00%	0.494
S <sub>60<math>\mu</math>m</sub> IRAS	S <sub>integ</sub> NVSS	0.00%	24.058	0.00%	5.802	0.00%	0.553
S <sub>100<math>\mu</math>m</sub> IRAS	S <sub>integ</sub> NVSS	0.00%	19.370	0.00%	5.394	0.00%	0.515

**Table 2.** High-resolution (A-configuration) and low-resolution (NVSS) radio flux densities are compared to infrared flux densities for all *IRAS* wavebands and the probability that no correlation exists between radio fluxes and *IRAS* fluxes, P(null), is given. *IRAS* fluxes are more closely related to low-resolution radio fluxes (NVSS) than high-resolution radio fluxes (A-configuration). The test statistics ( $\chi^2$ , Z and  $\rho$ ) show that the correlation between *IRAS* fluxes and NVSS fluxes is stronger for integrated NVSS fluxes than peak NVSS fluxes in all *IRAS* bands (the accuracy of the ASURV output is limited to 0.00%).

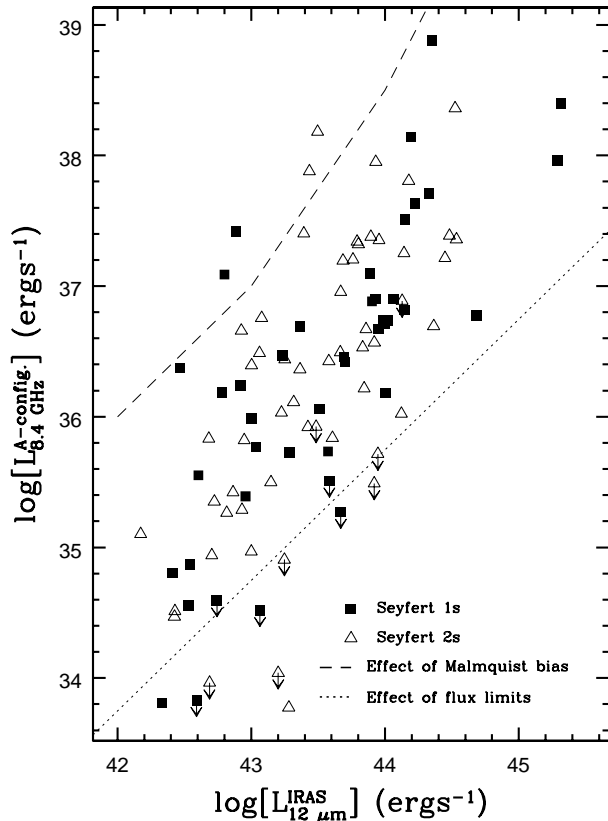


**Figure 6.** 8.4 GHz A-configuration luminosities are plotted against *IRAS* 12  $\mu$ m luminosities. The distribution of data points is restricted by the Malmquist bias and the observational flux limits, the remaining region is evenly filled and evidence for a correlation between the two variables is weak.

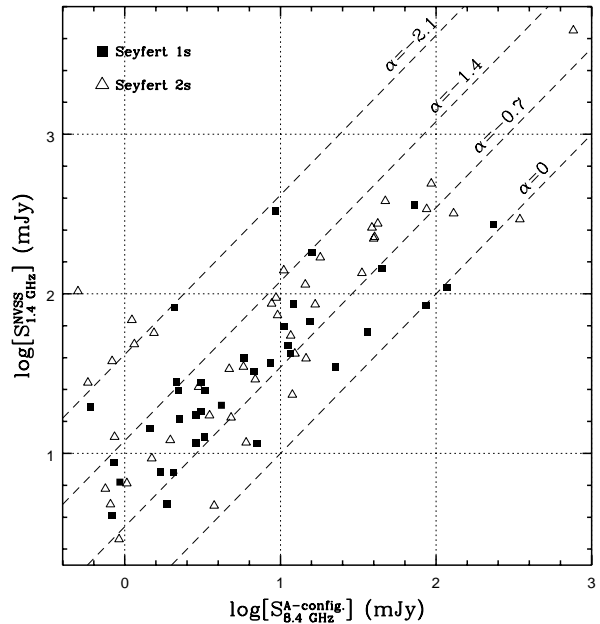


**Figure 8.** Peak VLA 1.4 GHz NVSS radio flux densities are plotted against 8.4 GHz A-configuration flux densities. Dashed lines indicate the flux relationships expected for various spectral indices; since NVSS observations measure a higher fraction of non-nuclear emission than 8.4 GHz A-configuration observations, the apparent spectral indices measured in this way provide lower limits to the true spectral indices of the nuclear components.

wavelengths are stronger for integrated NVSS fluxes than for peak NVSS fluxes (Table 2) means that a measurable fraction of *IRAS* emission, including mid-infrared emission, is generated by flux components larger than one third of the NVSS resolution i.e. 15 arcsecs (3.6 kpc at the mean redshift of the sample).

The most likely reason that NVSS fluxes are more closely related to *IRAS* fluxes than 8.4 GHz A-configuration

fluxes is that the VLA D and DnC configurations used for the NVSS survey are sensitive to low-brightness-temperature radio emission which is undetectable with the VLA A-configuration in snapshot mode at 8.4 GHz i.e. by radio emission with a brightness temperatures between around 0.14 K (NVSS limit) and 72 K (8.4 GHz A-configuration snapshot limit), or from flux components larger than 3.5 arcsec (1.6 kpc at the mean redshift of the sample). To some degree, the radio brightness-temperatures may be used to distinguish between emission with different physical origins e.g. the VLA in D and DnC configuration is sensitive to radio emission from normal H II regions and supernova remnants in nearby galaxies which is not usually compact enough to be detected by the VLA in A-configuration at 8.4 GHz (Condon et al. 1998).

Our results suggest that large-scale extra-nuclear emission regions, rather than compact nuclear regions, are primarily responsible for the correlation between NVSS and *IRAS* fluxes; stronger correlations between 8.4 GHz A-configuration fluxes and *IRAS* fluxes would be expected if compact regions dominate. We do not favour the interpretation that high-brightness-temperature radio emission from Seyfert nuclei is driven by compact nuclear starbursts (Terlevich et al. 1992), because such starbursts would be expected to make a significant contribution to *IRAS* fluxes. Note that for the majority of the sources we have detected, radio luminosity alone is not a good basis to rule out the possibility that they are caused by compact starbursts e.g. even though the 8.4 GHz A-configuration flux density of the well-known source ARP 220 would make it the 7th most luminous source in the sample, Smith et al. (1998) have provided strong evidence that its radio emission is dominated by a compact starburst.

Baum et al. (1993) identified three components which contribute to the radio emission from Seyfert galaxies; compact nuclear emission, kiloparsec-scale outflows and galactic disc emission. The correlation between radio emission and far-infrared emission is well known for normal spiral galaxies and starburst galaxies (de Jong et al. 1985; Helou, Soifer & Rowan-Robinson 1985; Condon & Broderick 1986; Condon & Broderick 1988; Bica & Helou 1990) and is explained by star-formation processes. Kiloparsec-scale radio outflows extending away from the galactic plane are found in half or more of Seyfert galaxies and are distinguished by their elongated morphology (Colbert et al. 1996). They are thought to be caused by AGN-driven jets but starburst-driven winds cannot be ruled out (Baum et al. 1993; Colbert et al. 1996; Colbert et al. 1998). It is difficult to determine whether the correlation between NVSS and *IRAS* fluxes is caused by kiloparsec-scale outflows or galactic disc emission because the radio to far-infrared flux ratio of kiloparsec-scale outflows is within the range found for normal spiral galaxies and starburst galaxies (Baum et al. 1993). Since it is an infrared-selected sample, the extended 12  $\mu\text{m}$  sample is likely to contain a high fraction of galaxies with infrared-bright discs and/or kiloparsec-scale outflows.

Our results are in agreement with those of previous authors who found that emission from the discs of Seyfert galaxies makes a significant contribution to their low-resolution radio fluxes (Edelson 1987; Wilson 1988; Rush, Malkan & Edelson 1996; Niklas 1997; Roy et al. 1998) e.g. Rush, Malkan & Edelson (1996) found that 50% of Seyfert

galaxies have extended flux components larger than 15 arcsec at 5 GHz and estimated that for these sources an average of 33% of the radio emission originates in the galactic disc. Rodriguez Espinosa, Rudy & Jones (1987) found that active nuclei may not be responsible for the bulk far-infrared emission from Seyfert galaxies at wavelengths longer than 30 microns. Our results support this interpretation and imply that it can be extended to 25 and 12  $\mu\text{m}$ , at least for mid-infrared-selected Seyferts, since correlations between radio fluxes and infrared fluxes at 25 and 12  $\mu\text{m}$  are much stronger for NVSS fluxes than for 8.4 GHz A-configuration fluxes.

If the *IRAS* fluxes of Seyfert galaxies are dominated by large-scale extra-nuclear regions rather than nuclear regions, *IRAS* colours do not provide a reliable indicator of the inclination of the circum-nuclear torus. Heisler, Lumsden & Bailey (1997) made the observation that Seyfert type 2 galaxies with hidden broad lines have ‘hot’ *IRAS* colours and inferred that they are sources whose tori have lower inclinations than other type 2 Seyferts, but an alternative explanation may be necessary (see §7). In addition, if *IRAS* colours are not dominated by emission from dust in the circum-nuclear torus, torus models are of limited importance in assessing selection biases in *IRAS*-selected samples i.e. even if the torus is optically-thick at mid-infrared wavelengths (§8) the extended 12  $\mu\text{m}$  sample may contain representative populations of type 1 and type 2 Seyferts.

Although *IRAS* fluxes seem to be dominated by emission regions which are less compact than those responsible for the 8.4 GHz A-configuration emission, at least some component of the *IRAS* flux at 25  $\mu\text{m}$  (and possibly at 12 and 60  $\mu\text{m}$ ) is correlated with high-brightness-temperature radio emission (§4.1). The reason that 8.4 GHz A-configuration fluxes are more closely correlated with 25  $\mu\text{m}$  fluxes than with 60  $\mu\text{m}$  and 100  $\mu\text{m}$  fluxes may be understood if high-brightness-temperature radio emission is more closely related with the hot gas and dust which dominates mid-infrared *IRAS* emission, than with the cooler gas and dust which dominates far-infrared *IRAS* emission. However, this does not explain why 8.4 GHz A-configuration fluxes are more closely correlated with 25  $\mu\text{m}$  fluxes than 12  $\mu\text{m}$  fluxes. The difference may be due to statistical limitations; Seyferts were selected at 12  $\mu\text{m}$ , the *IRAS* waveband in which their fluxes are faintest, and this means that the *IRAS* 12  $\mu\text{m}$  flux density distribution is the most severely truncated and correlations with *IRAS* 12  $\mu\text{m}$  fluxes are most difficult to quantify. If the difference is real, it may indicate that 12  $\mu\text{m}$  emission is less isotropic than 25  $\mu\text{m}$  emission; an explanation which is consistent with models of circum-nuclear tori which are optically-thick at 12  $\mu\text{m}$  (see §8.1).

The correlation between NVSS fluxes and 8.4 GHz A-configuration fluxes can be explained if, as expected, the compact components detected in A-configuration at 8.4 GHz also contribute to the NVSS fluxes. The fact that *IRAS* fluxes are only weakly related, if at all, to 8.4 GHz A-configuration fluxes can be explained if 8.4 GHz A-configuration fluxes are dominated by the active nucleus, NVSS fluxes contain a mixture of nuclear emission and extra-nuclear emission, and *IRAS* fluxes are dominated by extra-nuclear emission. This explanation is favoured by the fact that the correlation between NVSS fluxes and 8.4 GHz A-configuration fluxes is stronger for peak NVSS fluxes than integrated NVSS fluxes.

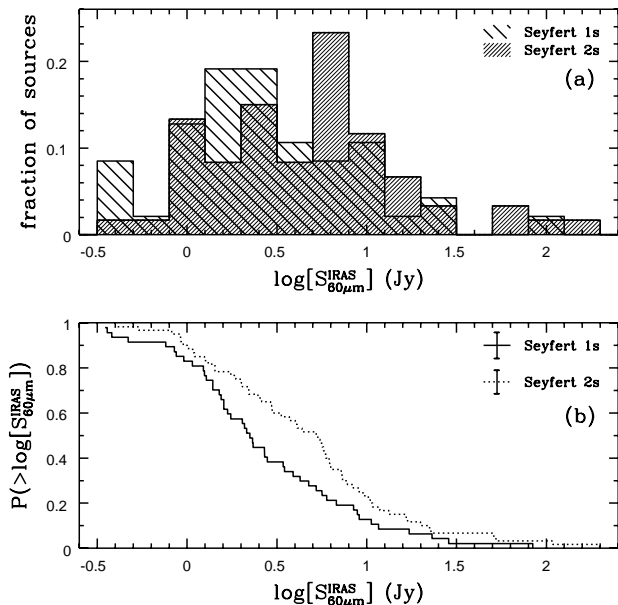


**Figure 9.** (a) Histograms showing the fractional *IRAS* 60  $\mu\text{m}$  flux density distributions and (b) the cumulative *IRAS* 60  $\mu\text{m}$  flux density distributions of 47 type 1 and 60 type 2 Seyferts in the extended 12  $\mu\text{m}$  sample. Type 2 Seyferts have significantly higher *IRAS* 60  $\mu\text{m}$  fluxes than type 1 Seyferts.

## 5 HOST GALAXIES

### 5.1 Large-scale emission from type 1 and type 2 Seyferts

Figure 9 shows the *IRAS* 60  $\mu\text{m}$  flux density distributions of type 1 and type 2 Seyferts in the extended 12  $\mu\text{m}$  sample. Type 2 Seyferts are significantly brighter than type 1 Seyferts. The probability of the null hypothesis, that the 60  $\mu\text{m}$  fluxes of the two Seyfert types are drawn at random from the same parent population, is: 4.66% (KS), 2.16% (Gehan’s, perm.), 1.93% (Gehan’s, hyper.), 4.10% (Logrank test) and 4.10% (Peto & Peto).

Figure 10 shows the NVSS integrated flux density distributions of type 1 and type 2 Seyferts in the sample. Type 2 Seyferts tend to have brighter NVSS fluxes, but the two flux distributions are statistically indistinguishable. The probability of the null hypothesis, that the NVSS integrated flux density distributions of the two Seyfert types are drawn at random from the same parent population, is: 19.45% (Gehan’s, perm.), 19.68% (Gehan’s, hyper.), 64.63% (Logrank test), 19.45% (Peto & Peto) and 19.65% (Peto & Prentice).

As a crude estimate of the strength of extended radio components we have calculated the quantity  $S_{\text{ext}}$  by subtracting 8.4 GHz A-configuration flux densities from integrated NVSS flux densities. Type 2 Seyferts tend to have higher  $S_{\text{ext}}$  values than type 1 Seyferts, but the difference between the  $S_{\text{ext}}$  distributions is only marginally significant. The probability of the null hypothesis, that  $S_{\text{ext}}$  values of type 1 and type 2 Seyferts are drawn at random from the same parent population, is: 11.31% (Gehan’s, perm.), 11.04% (Gehan’s, hyper.), 2.87% (Logrank test) and 2.87% (Peto & Peto).

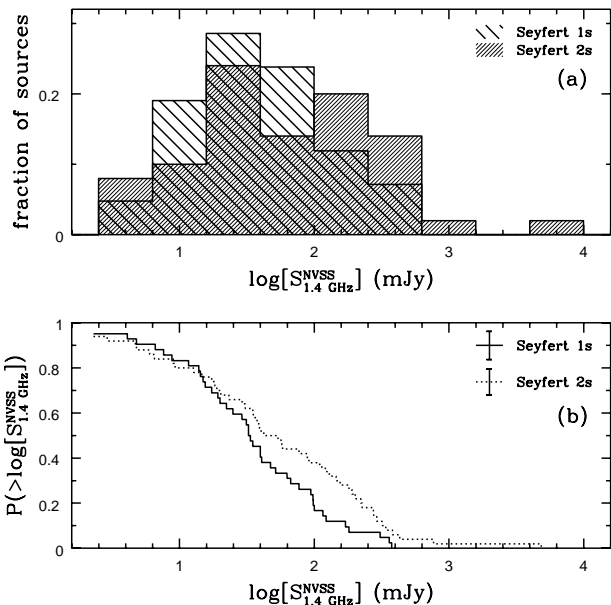


**Figure 10.** (a) Histograms showing the fractional NVSS integrated flux density distributions and (b) the cumulative NVSS integrated flux density distributions of 40 type 1 and 47 type 2 Seyferts in the extended 12  $\mu\text{m}$  sample. The NVSS integrated flux density distributions of the two Seyfert types are indistinguishable.

### 5.2 Implications: more extended emission in type 2 Seyferts ?

Our results, which suggest that type 2 Seyferts have brighter *IRAS* 60  $\mu\text{m}$  fluxes than type 1 Seyferts, are not expected according to the Seyfert unification model.

One possibility is that the extended 12  $\mu\text{m}$  Seyfert sample is biased against low-luminosity type 2 Seyferts; for example if *IRAS* emission is dominated by circum-nuclear tori which are optically-thick at 12  $\mu\text{m}$ , or if the population of newly-recognised type 2 Seyferts identified in Section 8.3 are low-luminosity sources. However, we do not favour this explanation because *IRAS* fluxes appear to be dominated by extra-nuclear emission regions (§4) and the sample appears to contain well-matched populations of type 1 and type 2 Seyferts (§8).

If extra-nuclear emission regions dominate *IRAS* fluxes, our results imply that they are brighter or more common in type 2 Seyferts than type 1 Seyferts. The marginally significant trend for type 2 Seyferts to produce more large-scale radio emission ( $S_{\text{ext}}$ ) than type 1 Seyferts favours this explanation. Note that differences between the integrated NVSS fluxes of type 1 and type 2 Seyferts will be hard to distinguish if NVSS fluxes contain a high fraction of AGN-related emission (§4.3). An excess in the extra-nuclear *IRAS* and NVSS emission of type 2 Seyferts supports claims that the host galaxies of type 2 Seyferts show excess of star-formation (Maiolino et al. 1995; Hunt & Malkan 1999) and an excess of wisps, filaments and dust lanes (Malkan, Gorjian & Tam 1998). Another alternative is that some starburst galaxies in the extended 12  $\mu\text{m}$  sample are misclassified as type 2 Seyferts.

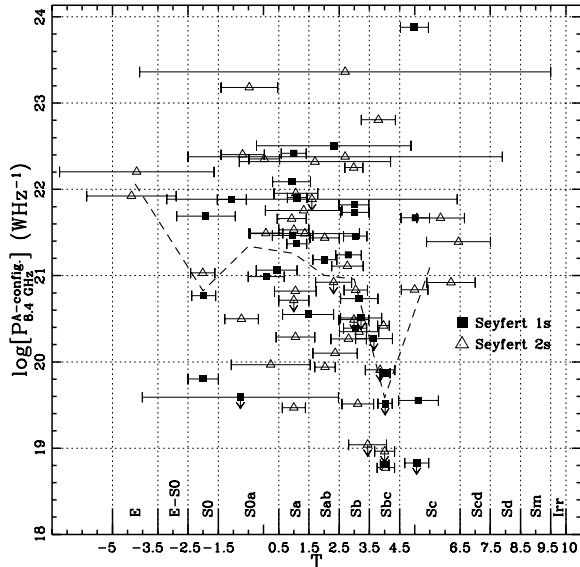


**Figure 11.** The 8.4 GHz VLA A-configuration radio powers of Seyferts from the extended 12  $\mu\text{m}$  sample are likely to be anti-correlated with the morphological type of the host galaxy,  $T$ , especially in the interval  $-1.5 < T < 4.5$ . A link between galaxy evolution and nuclear activity is indicated. Hubble types which correspond to the various ranges in  $T$  are shown on the x axis. The dashed line joins the mean values for each Hubble type (where the minimum value in a bin is an upper-limit, it is treated as a detection and the estimate of the mean is biased towards high values). The four most luminous sources, in order of decreasing luminosity, are: Markarian 231, Markarian 463, Markarian 348 and Markarian 533.

### 5.3 Host galaxy morphological types

Figure 11 shows how the 8.4 GHz A-configuration luminosities of the extended 12  $\mu\text{m}$  sample Seyferts are distributed according to the host morphological type,  $T$ . If radio luminosity upper-limits are considered, it is likely that there is an anti-correlation between  $T$  and radio power. The probability of the null hypothesis, that there is no correlation between host morphology (independent variable) and 8.4 GHz A-configuration luminosity, is: 0.78% (Cox proportional Hazard), 0.83% (Kendall’s Tau) and 0.87% (Spearman’s Rho). The anti-correlation is only statistically significant because of a group of late-type galaxies which were undetected in our radio survey, without the inclusion of luminosity upper-limits the probability of the null hypothesis is: 65.56% (Cox proportional Hazard), 8.59% (Kendall’s Tau) and 9.29% (Spearman’s Rho). On the other hand, the anti-correlation is highly significant for the 58 sources with morphological types in the range  $-1.5 < T < 4.5$  (Hubble types S0a to Sbc), for this sub-population the probability of the null hypothesis is: 0.15% (Cox proportional Hazard), 0.08% (Kendall’s Tau) and 0.12% (Spearman’s Rho). Note that the statistical tests used do not take into account uncertainties in morphological type.

Figure 12 shows how a measure of ‘radio-loudness’, the 8.4 GHz to *IRAS* 12  $\mu\text{m}$  flux ratio, is distributed according to the host morphological type,  $T$ . Even without the inclusion

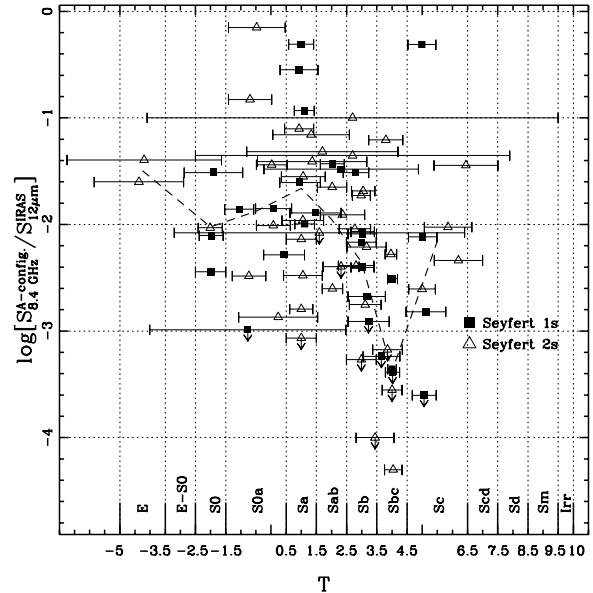


**Figure 12.** The ‘radio-loudness’ of Seyferts from the extended 12  $\mu\text{m}$  sample, as indicated by the 8.4 GHz VLA A-configuration to *IRAS* 12  $\mu\text{m}$  flux ratio, is likely to be anti-correlated with the morphological type of the host galaxy,  $T$ , especially in the interval  $-1.5 < T < 4.5$ . The dashed line joins the mean values for each Hubble type.

of flux density upper-limits, there is a marginally significant probability that there is an anti-correlation between  $T$  and the 8.4 GHz to *IRAS* 12  $\mu\text{m}$  flux ratio. The probability of the null hypothesis (no correlation) when radio flux density upper-limits are included is: 0.49% (Cox proportional Hazard), 0.15% (Kendall’s Tau) and 0.22% (Spearman’s Rho). Without the inclusion of radio flux density upper-limits the probability of the null hypothesis is: 14.15% (Cox proportional Hazard), 1.52% (Kendall’s Tau) and 2.19% (Spearman’s Rho). For sources in the range  $-1.5 < T < 4.5$  the probability of the null hypothesis is: 0.46% (Cox proportional Hazard), 0.04% (Kendall’s Tau) and 0.11% (Spearman’s Rho).

There is a statistically significant trend for galaxies with uncertain morphological types to host more powerful radio sources than other galaxies. There are 12 sources for which the uncertainty on the morphological type code is greater than unity, and the probability that the radio powers of these sources are drawn at random from the sample is low; 2.41% (Gehan’s, perm.), 0.78% (Gehan’s, hyper.), 3.46% (Logrank), 2.65% (Peto & Peto) and 1.48% (Peto & Prentice). The probability that the 8.4 GHz to *IRAS* 12  $\mu\text{m}$  flux ratio of these sources are drawn from the sample at random is: 3.68% (Gehan’s, perm.), 1.56% (Gehan’s, hyper.), 8.06% (Logrank), 3.86% (Peto & Peto) and 2.24% (Peto & Prentice). This trend may reflect observational difficulties in determining the morphological types of distant galaxies rather than a true link between morphological ambiguities and nuclear activity i.e. due to the Malmquist bias, distant sources are likely to be more powerful than nearby ones. Galaxies for which the uncertainty on the morphological type code is greater than unity tend to be more distant than other

sources in the sample, but this trend is of marginal significance. The probability that galaxies for which the uncertainty on the morphological type code is greater than unity have the same redshift distribution as the remaining sources is: 7.90% (Gehan's, perm.), 9.77% (Gehan's, hyper.), 3.09% (Logrank) and 3.09% (Peto & Peto).

#### 5.4 Implications: the strength of a nuclear radio source is related to host galaxy morphology.

There is a large degree of scatter in the formally significant anti-correlation between nuclear radio luminosity and host galaxy morphological type for the Seyferts in the extended 12  $\mu\text{m}$  sample, and its significance relies on luminosity upper-limits. A possible relationship between nuclear radio power and host galaxy morphology is highlighted by the sub-population of Sbc galaxies in the sample, which tend to have weaker nuclear radio sources than other types of galaxy. Evidence of an anti-correlation between the strength of nuclear activity and host galaxy morphology is clearest for sources with intermediate Hubble types (S0a to Sbc) and when a measure of radio-loudness, the radio to 12  $\mu\text{m}$  *IRAS* flux ratio, is considered instead of radio luminosity alone. The reason galaxies with morphological types earlier than S0a weaken the significance of the anti-correlation between radio power and host galaxy morphology may be related to the effects of mergers; the two galaxies classified as ellipticals (NGC 1143/4 and NGC 4922A/B) are multiple systems which are probably in the process of merging. The reason that galaxies with morphological types later than Sbc weaken the significance of the anti-correlation between radio power and galaxy morphology is unclear.

It is possible that our results are affected by bias; the selection criteria used to define the extended 12  $\mu\text{m}$  sample could mean that galaxies with low-luminosity AGN may satisfy the selection criteria simply because they have mid-infrared-bright discs, and this may introduce a bias against low-luminosity AGN in early-type galaxies. On the other hand, the trend for early-type galaxies to host more powerful radio sources than late-type galaxies is consistent with the fact that radio-loud AGN are usually found in elliptical galaxies and the fact that Seyfert nuclei are found preferentially in early-type host galaxies (Moles, Marquez & Perez 1995; Hunt & Malkan 1999). Previous studies have shown that galaxies with luminous bulges have the most powerful nuclei for both active galaxies (Whittle 1992; Ho 1999) and normal galaxies (Sadler, Jenkins & Kotanyi 1989; Kormendy & Richstone 1995). Taken together, recent results which link the mass of the central supermassive black hole of a galaxy to its bulge mass (Magorrian et al. 1998) and the radio power of its nucleus (Franceschini, Vercellone & Fabian 1998) suggest that a correlation between bulge mass and nuclear radio power is expected, and it is possible that the loose relationship between nuclear radio power and galaxy morphological type that we have found is indicative of a more fundamental relationship of this type.

In Section 4 we have shown that nuclear radio fluxes are more closely related to *IRAS* fluxes at 25  $\mu\text{m}$  than at any other *IRAS* wavelength and therefore our results are in good agreement with the anti-correlation between 25  $\mu\text{m}$  to 60  $\mu\text{m}$  *IRAS* flux ratios and morphological type found for extended 12  $\mu\text{m}$  Seyferts (Hunt & Malkan 1999).

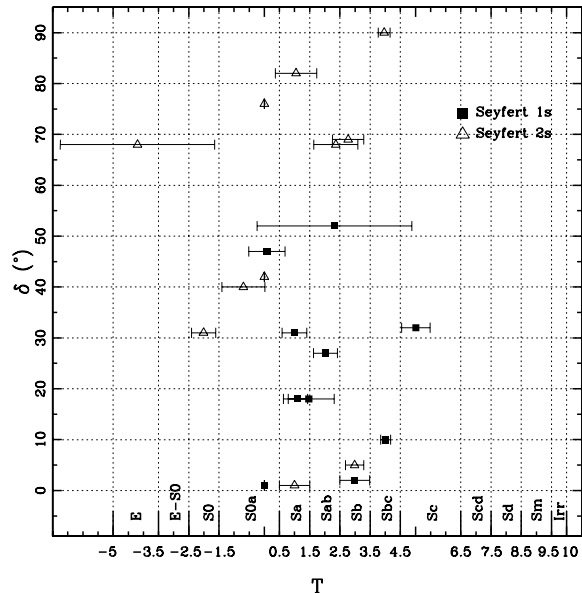


**Figure 13.** The difference between the position angles of the host galaxy major axes and the position angles of collimated nuclear radio structures,  $\delta$ , is plotted against the morphological type of the host galaxy,  $T$ . There is no apparent relationship between these two quantities.

If there is an anti-correlation between radio power and morphological type,  $T$ , one source which does not fit the general trend is the ultra-luminous infrared galaxy Markarian 231. This galaxy, which has an Sc morphology and a powerful, compact nuclear radio source, is probably the most luminous AGN in the local universe (Sanders et al. 1988). In Section 3.3 we considered the possibility that it contains a young radio source which may be in a particularly luminous phase of evolution.

#### 5.5 Host galaxy orientation

The difference between the position angle of the host galaxy major axis and the position angle of a collimated nuclear radio structure,  $\delta$ , is an indicator of how well the central AGN is aligned with the rotation axis of the host galaxy;  $\delta$  is 90 degrees for a central engine which is aligned with the galaxy rotation axis (the reliability with which  $\delta$  indicates the relative orientation of the AGN and the galactic plane decreases with galaxy inclination, but all galaxies for which values of  $\delta$  are available have an inclination greater than 30 degrees).

Figure 13 shows a plot of  $\delta$  versus host galaxy morphological type,  $T$ . We find an even distribution of  $\delta$  for the sample as a whole, suggesting that Seyfert central engines are randomly oriented with respect to their host galaxies. There is a marginally significant trend for type 2 Seyferts to show higher values of  $\delta$  than type 1 Seyferts, but this difference relies on a small number of sources. The probability of the null hypothesis, that the  $\delta$  distributions of type 1 and type 2 Seyferts are drawn at random from the same parent population, is: 14.20% (Gehan's, perm.), 13.83% (Gehan's, hyper.), 2.42% (Logrank) and 2.42% (Peto & Peto). There

is no obvious relationship between  $\delta$  and T. The probability that there is no correlation between  $\delta$  and T is: 90.66% (Cox proportional Hazard), 83.20% (Kendall’s Tau) and 71.16% (Spearman’s Rho).

### 5.6 Implications: no alignment between the central engine and the galactic disc.

Our results suggest that Seyfert central engines are randomly oriented with respect to their host galaxies. This result is in agreement with studies of individual sources whose 3-dimensional geometry can be measured accurately (e.g. Miyoshi et al. 1995) and other statistical studies using radio observations (Schmitt et al. 1997; Nagar & Wilson 1999). The main advantage of our study is that our sources are drawn from a homogeneously-selected sample.

Previous authors have found weak evidence that there is a deficiency of type 2 Seyferts with high values of  $\delta$ , the difference between the position angle of the host galaxy major axis and the position angle of a collimated nuclear radio structure (Schmitt et al. 1997; Nagar & Wilson 1999). In contrast to these results, we find a marginally significant deficiency of type 1 Seyferts with high values of  $\delta$ . Our result, together with those of previous authors, probably implies that there is no real difference between the  $\delta$  distributions of type 1 and type 2 Seyferts. The low-significance differences between the  $\delta$  distributions of type 1 and type 2 Seyferts which have been found to date may be the result of small-number statistics.

We find no evidence to support the weak trend for late-type Seyferts galaxies to favor larger values of  $\delta$  found by Wilson & Tsvetanov (1994) and Nagar & Wilson (1999).

## 6 NUCLEAR OUTFLOWS AND V-SHAPED EXTENDED EMISSION-LINE REGIONS

Mulchaey, Wilson & Tsvetanov (1996b) listed 15 Seyferts whose Extended Narrow-Line Regions (ENLRs) have a V-shaped morphology consistent with a cone-shaped nuclear radiation field. The following nine sources are common to the extended 12  $\mu\text{m}$  sample (the type of radio structure observed in A-configuration at 8.4 GHz is given in parenthesis): NGC 262=Markarian 348 (U), NGC 526A (S), NGC 1068 (L), NGC 1365 (A), Markarian 6 (L), NGC 4151 (L), NGC 4258=Markarian 766 (S), NGC 4388 (L) and NGC 7582 (D). Since emission-line images of all sources are not available it is unlikely that these are the only sources in the sample with V-shaped ENLRs.

Only one source with a V-shaped ENLR, Markarian 348, is unresolved at our resolution and this source is known to contain a linearly-aligned triple radio structure at higher resolution (Neff & de Bruyn 1983; Unger et al. 1984). Another source, which is only slightly resolved at 0.24 arcsec resolution, NGC 4528 (Markarian 766), is found to contain a slightly curving triple radio structure at higher resolution (unpublished MERLIN 5 GHz observations).

Sources known to contain V-shaped ENLRs have significantly larger radio sources than other types of source. Figure 14 shows the size distributions of the 9 extended 12  $\mu\text{m}$  Seyferts with V-shaped ENLRs compared to the remaining sources in the sample. The probability of the null hypothesis,

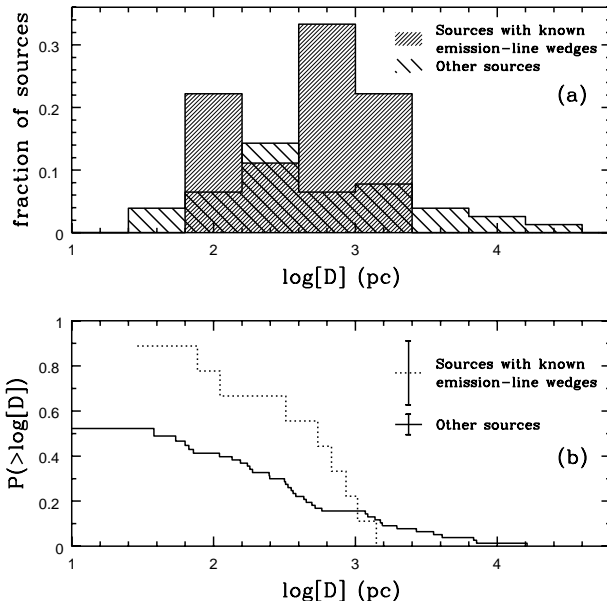


**Figure 14.** (a) Histograms showing the fractional radio size distributions of the 8 extended 12  $\mu\text{m}$  Seyferts which are known to contain V-shaped extended emission-line regions and were resolved and the 36 other resolved sources in the sample. (b) The cumulative size distributions of the 9 sources with V-shaped extended emission-line regions which were detected and the 77 other detected sources, as given by the Kaplan-Meier estimator where the y axis gives the probability that a source is larger than a given size. Sources known to have V-shaped extended emission-line regions are significantly larger than other sources.

that the size distributions of sources with known V-shaped ENLRs and other sources are drawn at random from the same parent population, is: 3.00% (Gehan’s, perm.), 1.80% (Gehan’s, hyper.), 0.73% (Logrank), 2.78% (Peto & Peto) and 3.78% (Peto & Prentice). For a bright subpopulation of 46 sources with 8.4 GHz A-configuration flux densities greater than 5 mJy/beam, the probability of the null hypothesis is: 21.46% (Gehan’s, perm.), 19.52% (Gehan’s, hyper.), 16.57% (Logrank), 22.04% (Peto & Peto) and 23.54% (Peto & Prentice).

Sources with V-shaped ENLRs are drawn from a nearby sub-population of the sample. The probability of the null hypothesis, that the redshift distributions of sources with known V-shaped ENLRs and other sources are drawn at random from the same parent population, is: 3.48% (Gehan’s, perm.), 1.39% (Gehan’s, hyper.), 0.44% (Logrank) and 0.44% (Peto & Peto). In fact, none of the sources with a known V-shaped ENLR is at a redshift higher than 0.020, and this probably reflects the scope of emission-line imaging surveys carried out to date and the difficulty of detecting faint extended emission-line regions in distant sources. For the sample as a whole, linear radio sizes tend to increase with redshift and therefore, if the fraction of nearby sources with both collimated radio structures and V-shaped ENLRs is similar for distant sources, the true significance of the difference in size between sources with V-shaped ENLRs and other Seyferts is likely to be greater than indicated by our comparison. Of a volume-limited sub-sample

of sources closer than redshift 0.020, V-shaped ENLRs have been found in four from nine sources with type L radio structures and two from nine sources with type S radio structures.

The connection between radio outflows and emission-line wedges is strengthened by radio observations of the six sources from the list of Mulchaey, Wilson & Tsvetanov (1996b) which are not found in the extended 12  $\mu\text{m}$  sample. Five of these sources have linear radio structures when observed at similar or identical resolution to our observations: Markarian 573 and NGC 5252 (Kukula et al. 1995), Circinus (Elmouttie et al. 1998), NGC 5728 (Schommer et al. 1988) and Markarian 78 (Pedlar et al. 1989). Only one (NGC 3281) has an unresolved radio structure (Ulvestad & Wilson 1989), and this means that elongated radio outflows indicative of radio jets are known for all but 3 sources from the list of Mulchaey, Wilson & Tsvetanov (1996b): NGC 1365, NGC 3281 and NGC 7582.

### 6.1 Implications: extended emission-line wedges are associated with radio outflows.

We have found that sources with emission-line wedges have significantly larger nuclear radio structures than other Seyferts. Given that extended emission-line wedges only appear to be present in around one in every eight Seyfert galaxies (Mulchaey, Wilson & Tsvetanov 1996b) and compact, collimated radio structures are found in around one in every five Seyfert galaxies (§3.2), the fact that these observational features often coincide, making comparisons between their orientations possible in the majority of cases (Wilson & Tsvetanov 1994; Nagar et al. 1999), is probably significant.

The main limitation of our comparison is that emission-line images are not available for all sources in the sample, and since sources with elongated radio structures were specifically targeted in early ENLR searches (radio maps were relied on to determine slit orientations using slit spectroscopy), we cannot rule out a bias against the identification of V-shaped ENLRs in sources with unresolved radio sources. The rate of occurrence of clear V-shaped ENLRs in the well-identified Early-type sample (Mulchaey, Wilson & Tsvetanov 1996b) implies that around 5 V-shaped ENLRs remain to be identified in the extended 12  $\mu\text{m}$  Seyfert sample. Since the sub-population of sources with V-shaped ENLRs is small, the addition of 5 sources with unresolved radio structures would be enough to make the radio size distribution of sources with V-shaped ENLRs match that of other Seyferts. On the other hand, sources with V-shaped ENLRs are more nearby than other types of Seyfert and this suggests that incompleteness is caused by difficulties in identifying V-shaped ENLRs in distant sources, rather than sources with unresolved radio structures. In fact, since distant sources tend to have larger linear sizes than nearby sources, a complete emission-line survey of the full sample may increase the significance of our result.

A relationship between extended radio sources and extended emission-line regions does not follow directly from the standard Seyfert unification model. According to the unification model a V-shaped ENLR is the result of a dusty circum-nuclear torus shadowing a central, isotropic uv source and the size and morphology of the central radio source is not an important parameter. One proposition which could reconcile our results with the unification model

is that large-scale collimated outflows are found preferentially in sources with luminous uv sources, in which ENLRs are most easily recognised. Correlations between radio power and [OIII] luminosity are known for Seyfert galaxies (de Bruyn & Wilson 1978; Whittle 1992) and resolved radio sources are, on average, more luminous than unresolved sources (§3.2). The fact that the radio structures of sources with V-shaped emission line regions are not significantly larger than other sources in a radio-bright sub-sample of sources supports this interpretation, but a true size difference would also be less significant in this smaller sample. An analysis of the emission-line fluxes of the sample, and further emission-line imaging, would help to determine whether our result can be explained by selection effects.

If there is a true connection between large radio sources and V-shaped extended emission-line regions, one possibility is that it is caused by interactions between nuclear outflows and the nuclear environment. Nuclear outflows of the size we have observed are unlikely to play a direct rôle in compressing/ionising extended emission-line regions because the ionised gas usually extends twice to five times as far from the active nucleus as the nuclear radio jets (Nagar et al. 1999). However, kiloparsec-scale radio outflows which are unobservable at high resolution are found in as many as half of all Seyferts (Colbert et al. 1996) and are thought to be caused by AGN-driven jets (Baum et al. 1993; Colbert et al. 1996; Colbert et al. 1998). The rôle of such outflows in evacuating and compressing ENLR gas would help explain the hollow ionisation cones found in certain sources (Pedlar et al. 1989; Wilson et al. 1993; Christopoulou et al. 1997).

Another possibility is that nuclear outflows ease the passage of ionising nuclear photons to extra-nuclear regions. Schulz (1988) suggested that extended narrow-line regions could be explained by holes in the narrow-line region caused by radio jets which push aside, or destroy, obscuring material. Recent HST observations support the idea that nuclear outflows evacuate channels in the narrow-line region and ease the passage of nuclear photons to extra-nuclear regions (Falcke, Wilson & Simpson 1998; Axon et al. 1998; Capetti et al. 1999). Wilson & Tsvetanov (1994) pointed out that radio ejecta are more tightly collimated than extended emission-line wedges and reasoned that long, narrow channels in the narrow-line region are not responsible for collimating the photon field which ionises the ENLR. However, the channels evacuated by narrow radio outflows are considerably wider than the radio jets themselves (Capetti et al. 1999), and even a relatively narrow outflow can cause a wide-angled uv-cone if the most optically thick region is close to the nucleus e.g. if circum-nuclear tori are created by nuclear outflows.

Lastly, a connection between radio outflows and extended emission-line regions could be related to source evolution. If Seyferts with large radio outflows are older than other types of Seyfert (§3.3) our results imply that extended emission-line wedges are also more likely to be found in old sources. Note that nuclear photons which travel to the ends of kiloparsec-scale emission-line regions are around  $1 \times 10^4$  years old and in Section 3.3 we discussed evidence that the largest (perhaps oldest) radio outflows from Seyferts are only around an order of magnitude older.

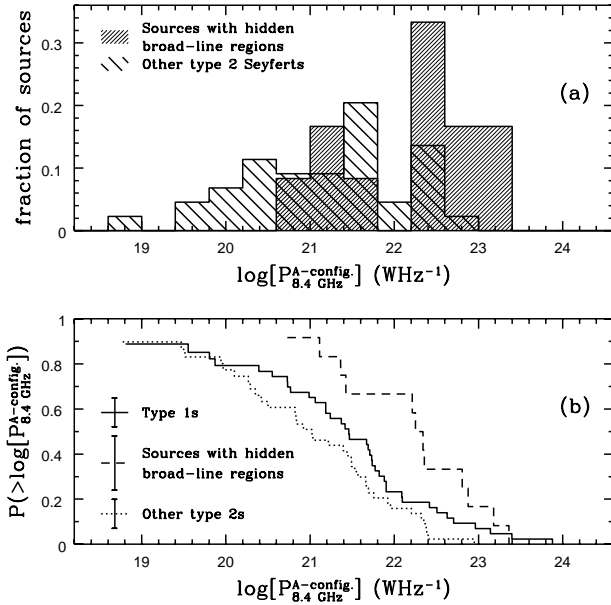


**Figure 15.** (a) The fractional 8.4 GHz A-configuration luminosity distributions of the 12 sources in the extended 12  $\mu\text{m}$  sample with known hidden broad line regions and the other 37 type 2 sources detected. (b) The cumulative 8.4 GHz A-configuration luminosity distributions of all observed sources (42 type 1s, 12 known hidden-broad-line sources and 44 other type 2s) as given by the Kaplan–Meier estimator, where the y axis gives the probability that a source is more luminous than a given radio power. Sources known to contain hidden broad line regions have more powerful nuclear radio sources than both type 1 sources and other type 2 sources.

## 7 SEYFERTS WITH HIDDEN BROAD-LINE REGIONS

Dopita et al. (1998) identified the following 14 sources in the extended 12  $\mu\text{m}$  sample which were classified as type 2 Seyferts by Rush, Malkan & Spinoglio (1993), and which are known to contain hidden broad lines (the type of radio structure observed in A-configuration at 8.4 GHz is given in parenthesis): F00198-7926 (unobserved), NGC 262=Markarian 348 (U), F01475-0475 (U), NGC 1068 (L), F04385-0828 (U), F05189-3524 (S), NGC 4388 (L), TOL 1238-364 (A), MCG-3-34-63 (S), Markarian 463 (L), F15480-0344 (U), IC 5063 (unobserved), F22017+0319 (L) and NGC 7674=Markarian 533 (L). Since this list has been drawn from the literature it is unlikely to be complete.

We find that sources with known hidden broad-line regions contain radio sources which are significantly more powerful than other Seyferts in the sample. A high fraction of the most radio luminous sources in the sample are either type 1 Seyferts or type 2 Seyferts with known hidden broad lines: of the 20 most radio luminous sources in the sample only 5 are not known to contain broad-line regions (Markarian 273, Markarian 6, F08572+3915, NGC 1125 and NGC 5256), and of the 20 sources with the highest 8.4 GHz to *IRAS* 12  $\mu\text{m}$  flux ratios only 2 are not known to contain broad-line regions (Markarian 6 and NGC 5506).

Figure 15 shows the 8.4 GHz A-configuration luminosity distributions of sources with known hidden broad-line

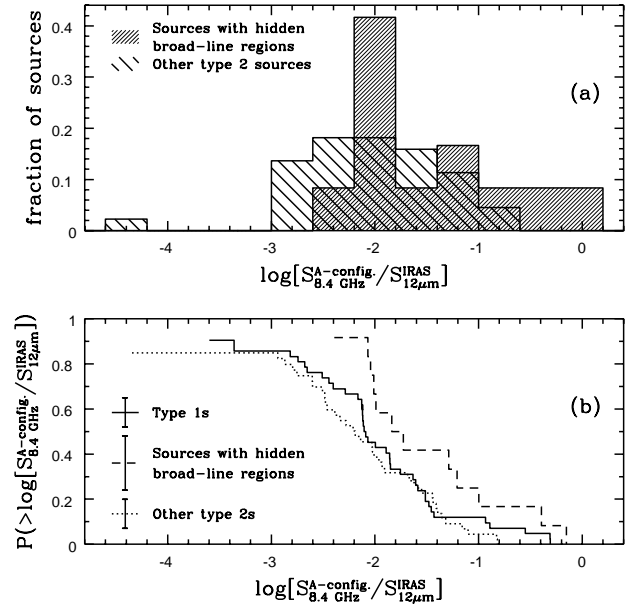


**Figure 16.** (a) The fractional distributions of the 8.4 GHz to *IRAS* flux ratio for the 12 sources in the extended 12  $\mu\text{m}$  sample with known hidden broad line regions and other 37 type 2 sources detected. (b) The cumulative distributions of the 8.4 GHz to *IRAS* flux ratios of all observed sources (42 type 1s, 12 known hidden-broad-line sources and 44 other type 2s) as given by the Kaplan–Meier estimator. Sources which are known to show hidden broad lines have a higher 8.4 GHz VLA A-configuration to *IRAS* 12  $\mu\text{m}$  flux ratios than both type 1 sources and other type 2 sources.

regions and other type 1 and type 2 Seyferts from the extended 12  $\mu\text{m}$  sample. Sources with known hidden broad-line regions are significantly more luminous than both type 1 Seyferts and type 2 Seyferts not known to show hidden broad-line regions. The probability of the null hypothesis, that the luminosities of type 1 sources and sources with known hidden broad-line regions are drawn at random from the same parent population, is: 3.02% (Gehan’s, perm.), 1.61% (Gehan’s, hyper.), 1.19% (Logrank test), 3.03% (Peto & Peto) and 2.85% (Peto & Prentice). The probability of the null hypothesis, that the luminosities of type 2 Seyferts not known to show hidden broad-line regions and type 2 Seyferts with known hidden broad-line regions are drawn at random from the same parent population, is: 0.15% (Gehan’s, perm.), 0.02% (Gehan’s, hyper.), 0.02% (Logrank test), 0.17% (Peto & Peto) and 0.10% (Peto & Prentice).

Figure 16 shows the 8.4 GHz A-configuration to *IRAS* flux ratio distributions of sources with known hidden broad-line regions and other type 1 and type 2 Seyferts in the sample. Sources with known hidden broad-line regions are significantly more ‘radio-loud’ than both type 1 Seyferts and type 2 Seyferts not known to show hidden broad-line regions. The probability of the null hypothesis, that the 8.4 GHz A-configuration to *IRAS* flux ratio distributions of type 1 sources and sources with known hidden broad-line regions are drawn at random from the same parent population, is: 3.20% (Gehan’s, perm.), 1.83% (Gehan’s, hyper.), 0.61% (Logrank test), 3.20% (Peto & Peto) and 3.49% (Peto



& Prentice). The probability of the null hypothesis, that the 8.4 GHz A-configuration to *IRAS* flux ratio distributions of type 2 sources not known to show hidden broad-line regions and type 2 sources with known hidden broad-line regions are drawn at random from the same parent population, is: 1.22% (Gehan's, perm.), 0.48% (Gehan's, hyper.), 0.15% (Logrank test), 1.24% (Peto & Peto) and 1.28 % (Peto & Prentice). These results are due to sources with known hidden broad-line regions having brighter radio fluxes, rather than fainter *IRAS* fluxes. The probability of the null hypothesis, that the 8.4 GHz A-configuration flux distributions of known hidden-broad-line sources and other type 1 or type 2 sources are drawn at random from the same parent population, is: 0.84% (Gehan's, perm.), 0.18% (Gehan's, hyper.), 0.12% (Logrank test), 0.83% (Peto & Peto) and 0.65% (Peto & Prentice).

Hidden broad-line regions have been identified in sources throughout the redshift range of the sample. The probability that the redshift distributions of sources with known hidden broad-line regions and all other Seyferts are drawn at random from the same parent population is: 27.37% (Gehan's, perm.), 30.00% (Gehan's, hyper.), 36.75% (Logrank test) and 36.75% (Peto & Peto). There is no evidence that the radio structures in sources with known hidden broad-line regions differ in size from other Seyferts. The probability that the radio sizes of sources with known hidden broad lines and all other Seyferts are drawn at random from the same parent population is: 27.93% (Gehan's, perm.), 25.82% (Gehan's, hyper.), 40.18% (Logrank test) and 33.51% (Peto & Peto) 32.38% (Peto & Prentice).

### 7.1 Implications: hidden broad-lines are associated with powerful radio emission.

Our results provide confirmation that type 2 Seyferts with known hidden broad lines have higher radio luminosities than other type 2 Seyferts, as claimed by Moran et al. (1992). Kay & Moran (1998) noted that Moran et al. did not compare carefully matched populations of type 1 and type 2 Seyferts, but our study suggests that this limitation does not invalidate the earlier result; we find the same trend using radio luminosity functions drawn from a single homogeneously-selected sample. The difference between the radio powers of sources with known hidden broad-line regions and other Seyferts in the sample suggests that the observation of hidden broad lines in type 2 Seyferts is not simply because they have low-inclination tori (Heisler, Lumsden & Bailey 1997); torus inclination should not affect radio power, especially for Seyfert 2s. In Section 4 we have suggested that *IRAS* flux ratios are better indicators of the relative strength of the nuclear and disc emission than of the torus inclination, and this interpretation is supported by the anti-correlation between 25  $\mu\text{m}$  to 60  $\mu\text{m}$  *IRAS* flux ratios and morphological type found for extended 12  $\mu\text{m}$  Seyferts (Hunt & Malkan 1999) which is hard to explain via torus inclination.

One explanation of our result is that observational limitations prevent the observation of hidden broad lines in sources with faint radio sources i.e. if broad-line luminosities are correlated with 8.4 GHz A-configuration luminosities the unidentified population of hidden-broad-line sources would have weak radio sources (Kay & Moran

1998). According to this explanation, hidden broad lines are only detectable where there is a high contrast between the AGN light and the galaxy light; the high fraction of hidden-broad-line sources among the most 'radio-loud' sources implies that, with sensitive enough observations, hidden broad lines should be detectable in around 80% of all type 2 Seyferts. If *IRAS* fluxes contain a mixture of 'hot' AGN emission and 'cooler' starburst/extra-nuclear emission (§4.3), Seyferts with powerful nuclei are expected to have the hottest *IRAS* colours, and this may explain why Seyferts with hidden broad lines have lower 60  $\mu\text{m}$  to 25  $\mu\text{m}$  *IRAS* flux ratios than other type 2 Seyferts (Heisler, Lumsden & Bailey 1997).

An alternative explanation of our result is that hidden-broad-line sources are intrinsically different from other Seyferts. The proposition that sources which show hidden broad lines have the brightest nuclei does not readily explain why they have smaller internal extinctions than other type 2 Seyferts (Heisler, Lumsden & Bailey 1997). In addition, the fact that hidden-broad-line sources have been identified throughout the redshift range of the sample suggests that their nuclei are not simply the brightest (most nearby) nuclei, but the most luminous. In fact, the identification of hidden broad lines does not always require high contrast between the AGN light and the galaxy light. For example, the optical spectrum of NGC 788 contains a significant fraction of starlight (Kay & Moran 1998); note however, that NGC 788 has a weak nuclear radio source.

Moran et al. (1992) used the excessive radio luminosities of Seyferts with hidden broad lines to suggest that there may be two types of Seyfert 2 galaxies; hidden type 1 objects and 'true' Seyfert 2 galaxies which lack broad emission lines. However, this explanation does not explain the fact that the population of sources with hidden broad lines is more powerful than the population of type 1 Seyferts. If the hidden-broad-line galaxies in the sample are well identified, they must be different from both 'true' type 2 Seyferts and type 1 Seyferts.

There is no evidence that the difference between hidden-broad-line sources and other Seyfert galaxies is related to radio outflows larger than tens of parsecs because the radio sizes and radio morphologies of the two populations are matched. However, closer to the active nucleus strong radio emission may indicate regions where electron scatters are abundant, or shock fronts which provide 'mirrors' for scattering nuclear photons.

## 8 SELECTION EFFECTS

The selection criteria of the sample studied can be the most important sources of systematic error in a statistical study of Seyfert galaxies. The lack of large samples in which type 1 and type 2 sources are represented equally has been an important governing factor for understanding the generic properties of Seyfert galaxies and has apparently lead to misleading comparisons of their radio properties. Since it has been selected from the *IRAS* catalogue, the extended 12  $\mu\text{m}$  sample is likely to contain Seyferts with higher than average star-formation rates, however, it is one of the largest well-defined samples of Seyfert galaxies available, and there is no evidence that either the type 1 and type 2 sources it

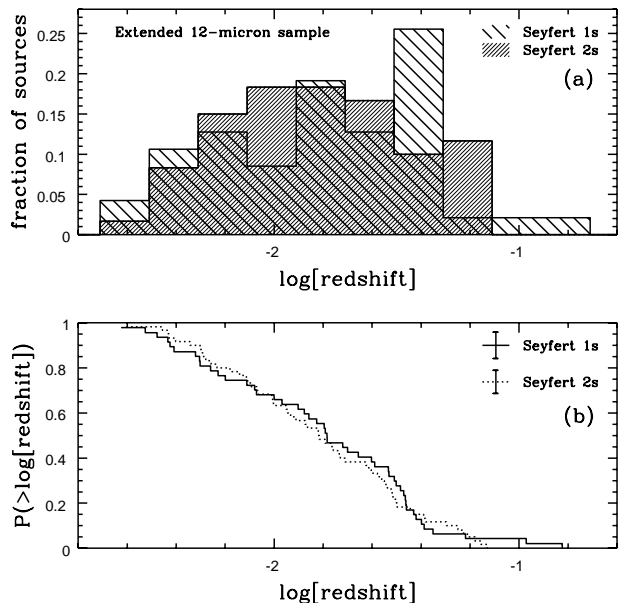


**Figure 17.** (a) Histograms showing the fractional redshift distributions of the 47 type 1 Seyferts and the 60 type 2 Seyferts in the extended 12  $\mu\text{m}$  Seyfert sample. (b) The cumulative redshift distributions. The fact that the two redshift distributions are likely to be drawn from the same parent population provides evidence that the sample has been selected in a way which will not bias the comparison of type 1 and type 2 sources.

contains are not of comparable bolometric luminosity. Here we attempt to identify its limitations and quantify any selection effects which could undermine our results by examining the selection criteria used.

### 8.1 The 12 $\mu\text{m}$ flux criterion

The 12  $\mu\text{m}$  AGN sample was selected according to the premise that an approximately constant fraction of the bolometric flux of quasars and both types of Seyferts is emitted in the *IRAS* 12  $\mu\text{m}$  band (Spinoglio & Malkan 1989). Contrary to this premise, models of optically-thick, geometrically-thin dusty tori predict that face-on tori (Seyfert 1s according to the unification model) may emit up to an order of magnitude more of their bolometric luminosity at mid-infrared wavelengths than edge-on tori (Pier & Krolik 1992; Granato & Danese 1994; Efstathiou & Rowan-Robinson 1995). Empirical evidence in favour of anisotropic mid-infrared emission from Seyferts is given by Heckman (1995) who compared small-aperture 10.6  $\mu\text{m}$  fluxes with [O III] fluxes and low-resolution 1.4 GHz fluxes for four samples of Seyferts and found evidence that the mid-infrared luminosities of type 1 Seyfert galaxies are 2 to 4 times higher than in type 2 Seyfert galaxies. According to this result, the extended 12  $\mu\text{m}$  Seyfert sample is expected to be biased against low-luminosity type 2 Seyferts because of the *IRAS* 12  $\mu\text{m}$  flux limit. In order to test this prediction we have compared the redshift distributions and 12  $\mu\text{m}$  flux distributions of type 1 and type 2 Seyferts in the sample.

The redshift distributions of different classes of object in a flux-limited sample provide indicators of whether they

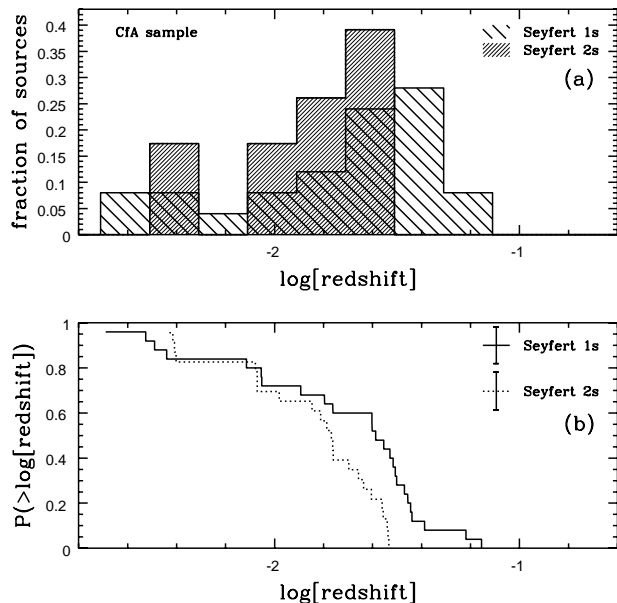


**Figure 18.** The fractional redshift distributions of the 26 type 1 Seyferts and the 22 type 2 Seyferts in the CfA sample indicate a possible bias against the selection of distant Seyfert 2s.

are equally luminous at the wavelength of selection; since the observed flux of an object of given luminosity falls proportionally with the square of its distance, differences between the luminosities of two classes of source at the wavelength of selection can easily produce mismatched redshift distributions. Therefore, if type 2 Seyferts are truly less luminous than type 1 Seyferts in the *IRAS* 12  $\mu\text{m}$  band, we expect them to be drawn from a smaller volume of space than type 1 Seyferts in the extended 12  $\mu\text{m}$  sample.

Figure 17 shows the redshift distributions of the two Seyfert types in the extended 12  $\mu\text{m}$  sample. The two types are equally distributed according to redshift. The probability of the null hypothesis, that the redshift distributions of the two Seyfert types are drawn at random from the same parent population, is: 94.48% (KS test), 83.84% (Gehan's perm.), 83.86% (Gehan's hyper.), 68.70% (Logrank test) and 68.70% (Peto & Peto). The mean redshift of Seyfert 1s is  $0.024 \pm 0.004$  and that of Seyfert 2s is  $0.022 \pm 0.002$ : the larger difference between the mean redshifts of type 1 and type 2 objects in the extended 12  $\mu\text{m}$  AGN sample noted by Rush, Malkan & Spinoglio (1993) and Hunt & Malkan (1999) is due to the inclusion of the 5 radio-loud sources we have excluded in Paper I (Thean et al. 2000a). The redshift distributions show no evidence of the identification bias against faint Seyfert 2s discussed in Section 8.3; note that a bias against faint type 2 Seyferts acts in the opposite sense to that required to reconcile the observed redshift and 12  $\mu\text{m}$  flux density distributions with the results of Heckman (1995).

For comparison with the extended 12  $\mu\text{m}$  Seyfert sample, Figure 18 shows the redshift distributions of the CfA Seyfert sample (Huchra & Burg 1992). The CfA Seyfert sample has the advantage of being selected spectroscopically without the use of (biased) catalogues of AGN, however, the redshift distributions the two Seyfert types in this sample

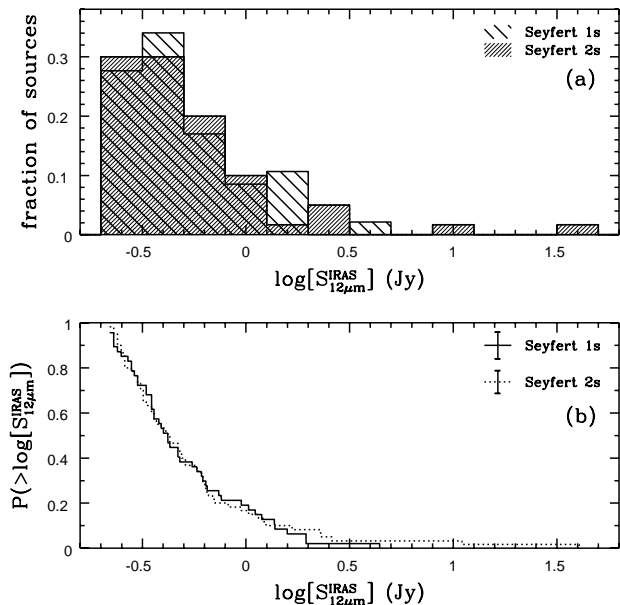


**Figure 19.** (a) Histograms showing the fractional *IRAS* 12  $\mu\text{m}$  flux density distributions of the 47 type 1 Seyferts and the 60 type 2 Seyferts in the extended 12  $\mu\text{m}$  sample. (b) The cumulative 12  $\mu\text{m}$  flux density distributions. The flux density distributions are well matched and together with the redshift distributions, this implies that the two Seyfert types are equally luminous at the wavelength of selection.

appear to differ. The probability of the null hypothesis, that the two Seyfert types are drawn at random from the same parent population, is: 5.9% (KS test) 8.4% (Gehan’s perm.), 7.9% (Gehan’s hyper.), 0.4% (Logrank test) and 0.4% (Peto & Peto). These test results are inconclusive, but the sense of the difference in the two populations and the results of the Logrank and Peto & Peto tests are suggestive of a bias against distant type 2 Seyferts. This type of bias could be explained by the criteria used to define the CfA sample; at the wavelength of selection Seyfert type 1 nuclei are more luminous than type 2 nuclei and can account for a significant fraction of the light of the host galaxy, in addition, broad emission line profiles make distant type 1 sources easier to identify (Kukula et al. 1995).

From their matched redshift distributions, we have inferred that type 1 and type 2 Seyferts in the extended 12  $\mu\text{m}$  sample are equally luminous in the *IRAS* 12  $\mu\text{m}$  band (8.5  $\mu\text{m}$  to 15  $\mu\text{m}$ ). This is supported by the fact the *IRAS* 12  $\mu\text{m}$  flux density distributions of type 1 and type 2 Seyferts in the sample are also well matched (see Fig. 19). The probability of the null hypothesis, that the *IRAS* 12  $\mu\text{m}$  fluxes of type 1 and type 2 Seyferts are drawn at random from the same parent population, is: 98.31% (KS test), 100.00% (Gehan’s perm.), 100.00% (Gehan’s hyper.), 76.12% (Logrank) and 76.12% (Peto & Peto).

In summary, our results suggest that the *IRAS* 12  $\mu\text{m}$  emission from type 1 and type 2 Seyferts is of roughly equal strength. They are in good agreement with those of Fadda et al. (1998) who argued against early models of compact, very optically-thick tori. A possible explanation for the low small-aperture 10.6  $\mu\text{m}$  to 1.4 GHz single-dish flux ratios

of type 2 Seyferts in the extended 12  $\mu\text{m}$  sample (Heckman 1995) is that type 2 Seyferts have brighter non-nuclear radio fluxes (§5.2); note that the small-aperture 10.6  $\mu\text{m}$  to [OIII] flux ratios of type 1 and type 2 Seyferts from the extended 12  $\mu\text{m}$  sample are indistinguishable.

## 8.2 Infrared colour criteria

In Section 5.1 we showed that the *IRAS* 60  $\mu\text{m}$  flux distributions of the type 1 and type 2 Seyferts in the extended 12  $\mu\text{m}$  sample are different, and this means that the colour criteria used to define the sample could be a source of bias. The mid- to far-infrared colour distributions are not significantly truncated by the explicit infrared colour criterion used to define the sample ( $S_{12\mu\text{m}}/S_{60\mu\text{m}} \leq 2$  or  $S_{12\mu\text{m}}/S_{100\mu\text{m}} \leq 1$ ) and these are unlikely to cause a significant bias. However, a further selection criterion, which was used in order to ensure real *IRAS* detections, requires all sources to have moderate or high flux quality flags on 60  $\mu\text{m}$  or 100  $\mu\text{m}$  fluxes as well as on 12  $\mu\text{m}$  fluxes. This acts as a ‘hidden colour criterion’ and tends to bias the sample against faint sources with high mid- to far-infrared flux ratios i.e. the *IRAS* sensitivity at both 60  $\mu\text{m}$  and 100  $\mu\text{m}$  is lower than that at 12  $\mu\text{m}$  so, in order to be selected, sources near the 12  $\mu\text{m}$  flux limit must have lower mid- to far-infrared flux ratios than required by the explicit infrared colour criterion. Taking  $3\text{-}\sigma$  detection thresholds\* at 12  $\mu\text{m}$ , 60  $\mu\text{m}$  and 100  $\mu\text{m}$  of 0.21 Jy, 0.26 Jy and 0.90 Jy respectively, the ‘hidden colour criterion’ requires that sources at the flux limit must satisfy the criterion  $S_{12\mu\text{m}}/S_{60\mu\text{m}} \leq 0.85$  or  $S_{12\mu\text{m}}/S_{100\mu\text{m}} \leq 0.24$ . Since type 1 Seyferts are more likely to have high mid- to far-infrared flux ratios than type 2 Seyferts, the hidden colour criterion can result in a bias against weak type 1 Seyferts. For sources with *IRAS* 12  $\mu\text{m}$  flux densities brighter than 0.52 Jy ( $\sim 40\%$  of the sample) the *IRAS* 60  $\mu\text{m}$  sensitivity is enough to detect any sources which would satisfy the  $S_{12\mu\text{m}}/S_{60\mu\text{m}} \leq 2$  condition (no sources in the AGN sample fail the  $S_{12\mu\text{m}}/S_{60\mu\text{m}} \leq 2$  condition and are selected on the basis of their 100  $\mu\text{m}$  flux density). Of these bright sources, only two do not satisfy the ‘hidden colour criterion’, and both are type 1 Seyferts (F05563-3820 and MK704). If a similar fraction of faint sources are missing from the full sample, around 3 faint Seyferts (most likely type 1s) which have the 12  $\mu\text{m}$  flux densities above the flux limit will have been omitted because they have high mid- to far-infrared flux ratios.

## 8.3 The AGN identification procedure

One limitation of the extended 12  $\mu\text{m}$  AGN sample is that AGN were identified by cross-referencing with the literature without a complete and homogeneous spectroscopic identification procedure. Although redshifts are available for 98% of the extended 12  $\mu\text{m}$  galaxy sample, the quality of the spectroscopy used to provide them is insufficient to identify Seyferts with weak emission lines. For this reason, Seyferts in the extended 12  $\mu\text{m}$  sample can be difficult to identify. A number of sources were not recognised as AGN at the time

\* Average noise values were taken from the *IRAS* website ([www.ipac.caltech.edu/ipac/iras/iras\\_mission.html](http://www.ipac.caltech.edu/ipac/iras/iras_mission.html)).

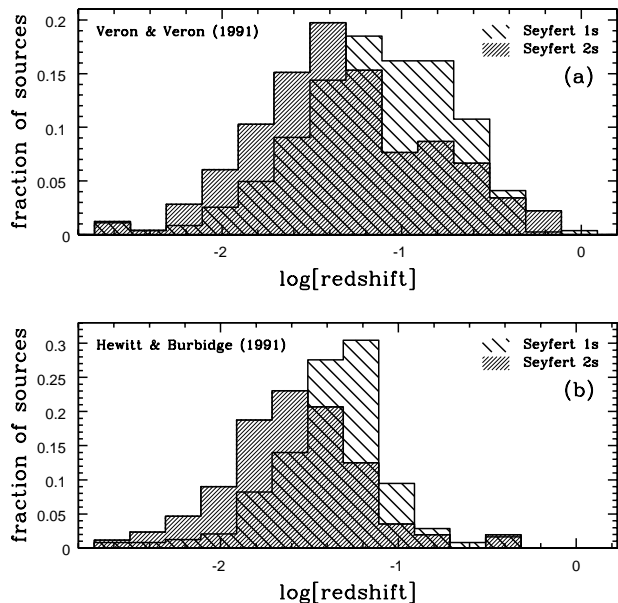


**Figure 20.** Histograms showing the fractional redshift distributions of the two Seyfert types in (a) Veron & Veron (1991) and (b) Hewitt & Burbidge (1991), two of the catalogues used to identify AGN in the extended 12  $\mu\text{m}$  sample. The relative fraction of Seyfert 1s in these catalogues increases steadily with redshift indicating a bias against distant Seyfert type 2 sources. There are a total of 827 Seyfert 1s and 496 Seyfert 2s listed in Veron & Veron (1991) and 243 Seyfert 1s and 256 Seyfert 2s listed in Hewitt & Burbidge (1991).

Rush, Malkan & Spinoglio (1993) defined the AGN sample. By cross-referencing the extended 12  $\mu\text{m}$  sample with the NED, Hunt & Malkan (1999) found 29 galaxies which were classified as ‘normal galaxies’ or ‘high-far-infrared’ galaxies by Rush et al., but which are classified as Seyferts in the NED. We have identified 38 such sources by the same procedure (see Appendix E); note that Hunt et al. also found that 22 of Seyferts identified by Rush et al. are not classified as Seyferts in the NED.

From  $V/V_{\text{max}}$  completeness tests, Rush et al. initially suspected that some weak type 1 Seyferts remained to be identified in the sample, however, nearly all of the newly-recognised Seyferts are type 2 sources. This result is in the sense predicted by Barcons et al. (1995) who estimated that up to 20% of the weak Seyfert 1s and 50% of the weak Seyfert 2s were missing from the sample. The most likely reasons that the majority of the newly-recognised Seyferts are type 2s is that AGN search techniques can favour the discovery of Seyfert 1s and Seyfert 2s with faint emission lines are hard to identify with low quality optical spectra. Figure 20 shows the redshift distributions of type 1 and type 2 Seyferts from two of the AGN catalogues used to identify AGN in the extended 12  $\mu\text{m}$  sample. A bias against distant (faint) type 2 Seyferts is evident in both catalogues. The ratio of the number of Seyfert 1s to the number of Seyfert 2s contained in these catalogues increases steadily with redshift and there is an extremely low probability that the redshift distributions of type 1 and type 2 Seyferts are drawn at random from the same parent population:  $2 \times 10^{-14}\%$  (KS) for Veron-Cetty &

Veron (1991) and  $8 \times 10^{-10}\%$  (KS) for Hewitt & Burbidge (1991).

The radio properties of the newly-identified type 2 Seyferts in the sample may affect several of our results, particularly if they are low-luminosity sources. For example, correlations between radio power and forbidden-line luminosities (de Bruyn & Wilson 1978; Whittle 1992) may mean that we have over-estimated the strengths of type 2 Seyferts. The complete identification of Seyferts from the extended 12  $\mu\text{m}$  galaxy sample and follow-up radio observations would be useful for improving the accuracy of our analysis.

## 9 SUMMARY

The main results of our analysis may be summarised as follows:

- Eighty-five of the 98 Seyferts from the extended 12  $\mu\text{m}$  AGN sample observed were detected by the VLA in A-configuration at 8.4 GHz. They showed a range of radio morphologies; roughly 50% were unresolved, 20% were slightly-resolved, 10% had two components, 10% had two or more linearly-aligned components and 10% had diffuse or ambiguous morphologies.
- There is no significant difference between the luminosities of compact radio components in type 1 and type 2 Seyferts. This result is consistent with the Seyfert unification model and suggests that the central engines of each type of Seyfert are similar.
- There is no significant difference between the sizes or morphologies of compact radio components in type 1 and type 2 Seyferts in the sample. This result is consistent with the Seyfert unification model and suggests that each type of Seyfert has a similar capacity to produce extended radio outflows (our comparison is probably insensitive to the effects of orientation).
- There is a significant correlation between radio power and radio size for type 2 Seyferts which show evidence of collimated nuclear radio sources. The same correlation is not shown by type 1 Seyferts.
- The *IRAS* emission from infrared-bright Seyfert galaxies is probably dominated by kiloparsec-scale emission regions, possibly star-forming regions.
- There is evidence of a correlation between host galaxy morphology and nuclear radio power, with early-type galaxies showing more luminous radio cores.
- Collimated nuclear radio sources appear to be randomly oriented with respect to the galactic plane.
- The nuclear radio sources of Seyferts with known V-shaped extended emission-line regions, indicative of ‘ionisation cones’, are larger than other sources in the sample.
- The nuclear radio sources of Seyferts with known hidden broad-line regions are more powerful than other types of Seyfert.
- The extended 12  $\mu\text{m}$  sample appears to contain matched populations of type 1 and type 2 Seyfert galaxies.

## 10 ACKNOWLEDGMENTS

AHCT would like to acknowledge the receipt of a studentship from the Particle Physics and Astronomy Re-

search Council and a visit funded by the STScI visitor program. Part of this research was supported by the European Commission, TMR Programme, Research Network Contract ERBFMRXCT96-0034 ‘‘CERES’’. We have made use of NASA’s Astrophysics Data System Abstract Service, the NASA/IPAC Extragalactic database (NED), which is operated by the Jet Propulsion Laboratory, and ASURV Rev 1.1 (Lavalley, Isobe & Feigelson 1992), which implements the methods presented in Feigelson & Nelson (1985) and Isobe, Feigelson & Nelson (1986). We thank the referee, R. Antonucci, for helpful comments.

## APPENDIX A: ARCHIVE DATA

### A1 Host galaxy morphologies

Morphological classifications were available in the LEDA for 78 galaxies from the extended 12  $\mu\text{m}$  Seyfert sample and are given in Table A1 which is arranged as follows; *Column 1*: Galaxy name; *Column 2*: Galaxy type,  $T_{\text{Sy}}$ . *Column 3*: Hubble type,  $T_{\text{Hubble}}$ , as obtained from the NED; *Column 4*: Morphological type code, T, and its associated uncertainty,  $\Delta T$ , as obtained from the LEDA. Galaxy morphological types in the LEDA are codified using the continuous parameter T following the methods outlined in The Third Reference Catalogue of Bright Galaxies (RC3) (de Vaucouleurs et al. 1991), low values of T correspond to early-type galaxies (Fig. 11 shows the ranges in T which correspond to the various Hubble types). *Column 5*: Position angle of the galaxy major axis, PA, in degrees; *Column 6*: Inclination of the galaxy,  $i$ , in degrees.

### A2 NVSS components

Table A2 gives the VLA D and DnC configuration 1.4 GHz radio flux densities obtained from the NVSS for 92 of the 113 radio-quiet sources from the extended 12  $\mu\text{m}$  sample. NVSS counterparts within 10 arcsec of the A-configuration positions are found for 85 of the 87 sources at declinations north of  $-40$  degrees for which A-configuration positions are available (there is less than a 0.2% probability of finding a NVSS source within 10 arcsec of an arbitrary position in the sky). Seven out of ten of the sources north of declination  $-40$  degrees and without A-configuration positions have NVSS counterparts within 20 arcsec of the IRAS position (there is a 0.5% probability of finding a NVSS source within 20 arcsec of an arbitrary position in the sky). Sixteen sources are south of  $-40$  degrees declination in a region of sky not covered by the NVSS. Table A2 is arranged as follows; *Column 1*: Galaxy name; *Column 2*: Galaxy type, starbursts (s) and LINERs (L) have been excluded from our analysis; *Column 3 and 4*: Right ascension and declination of the NVSS components determined from Gaussian fits; *Column 5*: The separation of the NVSS component position and the VLA 8.4 GHz A-configuration or IRAS position,  $\theta_{\text{sep}}$ , in arcseconds. The rms uncertainties in right ascension and declination for the NVSS are 0.3 arcsec for strong point sources ( $S > 30$  mJy/beam) and 5 arcsec for the faintest sources detectable ( $S = 2.5$  mJy/beam). Sources whose NVSS counterparts were found by searching on IRAS positions rather than 8.4 GHz VLA A-configuration positions are denoted

Galaxy	$T_{\text{Sy}}$	$T_{\text{Hubble}}$	$T \pm \Delta T$	PA ( $^\circ$ )	$i$ ( $^\circ$ )
NGC262=Mrk348	2	S0a	$-0.472 \pm 0.935$	–	14
NGC424=TOL0109	2	S0a-R	$0.077 \pm 0.561$	60	63
NGC526A	1	S0	$-1.906 \pm 0.967$	–	58
NGC513	2	Sc	$6.200 \pm 0.800$	75	61
Mrk1034	1	Sab	$2.320 \pm 2.557$	117	0
MCG-3-7-11	1	Sc	$5.015 \pm 0.469$	2	42
NGC931=Mrk1040	1	Sbc	$3.651 \pm 0.608$	–	75
NGC1056=Mrk1183	2	Sa	$1.000 \pm 0.384$	160	56
NGC1068	2	Sb	$2.985 \pm 0.300$	70	31
NGC1125	2	S0a	$0.024 \pm 0.506$	–	60
NGC1143/4	2	E	$-4.195 \pm 2.553$	130	48
MCG-2-8-39	2	SBa	$1.000 \pm 0.500$	10	50
NGC1194	2	S0a	$-0.730 \pm 0.556$	140	51
NGC1241	2	SBb	$3.048 \pm 0.389$	145	49
NGC1320=Mrk607	2	Sa	$1.053 \pm 0.641$	45	70
NGC1365	1	SBb	$3.165 \pm 0.615$	32	55
*NGC1566	1	SBbc	$4.008 \pm 0.142$	60	42
Mrk618	1	SBb	$2.989 \pm 0.494$	85	41
NGC1667	2	SBc	$4.996 \pm 0.442$	20	39
*E33-G2	2	S0	$-2.200 \pm 1.800$	10	20
MCG-5-13-17	1	S0a-M	$0.086 \pm 0.597$	160	53
E253-G3	2	S?	$1.600 \pm 4.800$	108	44
Mrk6	2	S0a	$-0.693 \pm 0.712$	130	51
Mrk9	1	S0	$-2.000 \pm 0.500$	–	35
Mrk79	1	SBb	$3.034 \pm 0.386$	–	4
NGC2639	1	Sa	$0.997 \pm 0.412$	140	40
NGC2992	2	Sa-M	$0.930 \pm 0.481$	15	76
NGC3079	2	SBc	$6.447 \pm 1.055$	165	81
NGC3227	1	SBa-M	$1.472 \pm 0.842$	155	46
NGC3511	1	SBc-M	$5.065 \pm 0.393$	76	70
NGC3516	1	S0-R	$-1.977 \pm 0.396$	–	34
M+0-29-23	2	Sb	$2.989 \pm 0.494$	–	32
NGC3660	2	SBbc-R	$3.852 \pm 0.487$	115	36
NGC3982	2	SBb	$3.118 \pm 0.525$	–	29
NGC4051	1	SBbc	$4.002 \pm 0.142$	135	34
UGC7064	1	SBb	$3.226 \pm 0.682$	–	0
NGC4151	1	SBab-R	$2.025 \pm 0.397$	50	38
Mrk766	1	SBa	$0.958 \pm 0.670$	–	21
NGC4388	2	Sb	$2.773 \pm 0.519$	92	74
NGC4501	2	Sb	$3.440 \pm 0.630$	140	57
NGC4579	1	SBb	$2.807 \pm 0.421$	95	37
NGC4593	1	SBb-M	$3.026 \pm 0.382$	55	45
NGC4594	1	Sa	$1.101 \pm 0.330$	89	59
NGC4602	1	SBbc	$4.020 \pm 0.236$	81	70
Mrk231=UGC8058	1	Sc	$4.988 \pm 0.462$	10	42
NGC4922A/B	2	E-M	$-4.370 \pm 1.482$	–	14
NGC4941	2	SBab	$2.365 \pm 0.731$	15	51
NGC4968	2	S0	$-2.010 \pm 0.399$	56	61
NGC5005	2	SBbc	$3.965 \pm 0.194$	65	60
NGC5033	1	Sc	$5.120 \pm 0.658$	170	67
MCG-3-34-63	2	S?	$2.700 \pm 5.200$	–	72
NGC5135	2	SBab	$2.316 \pm 0.597$	–	21
NGC5194=M51	2	Sbc-M	$4.041 \pm 0.290$	163	46
MCG-6-30-15	1	E-S0	$-0.767 \pm 3.242$	116	54
NGC5256=Mrk266	2	Sab	$1.700 \pm 2.500$	–	32
I4329A	1	S0a	$-1.051 \pm 0.480$	45	72
NGC5347	2	SBab-R	$2.029 \pm 0.336$	130	38
Mrk463	2	S?	$2.700 \pm 6.800$	–	60
NGC5506	2	Sa	$1.326 \pm 1.266$	91	74
NGC5548	1	S0a-R	$0.428 \pm 0.675$	110	34
NGC5929	2	Sa-M	$1.362 \pm 1.808$	–	16
NGC5953	2	S0a-M	$0.236 \pm 1.309$	169	43
MCG-2-40-4	2	Sa	$1.000 \pm 0.500$	120	38
*E141-G55	1	Sc	$5.200 \pm 0.000$	50	48
*NGC6860	1	Sb	$2.961 \pm 0.463$	34	56
NGC6890	2	SBb	$2.811 \pm 0.587$	152	36
*15063	2	S0a	$-1.019 \pm 0.660$	116	48
UGC11680=Mrk897	2	Sc-M	$5.856 \pm 0.788$	70	48
NGC7130=I5135	2	Sa	$1.065 \pm 0.723$	–	22
NGC7172	2	Sa	$1.050 \pm 0.685$	100	56
NGC7213	1	Sa	$0.924 \pm 0.624$	–	28
NGC7314	1	SBbc	$4.017 \pm 0.164$	3	64
NGC7469	1	SBa	$1.113 \pm 0.321$	125	45
NGC7496	2	SBb	$3.159 \pm 0.647$	–	18
NGC7582	2	SBab	$2.020 \pm 0.485$	157	63
NGC7590	2	Sbc	$4.003 \pm 0.328$	36	67
NGC7603=Mrk530	1	Sb	$3.018 \pm 0.471$	165	49
NGC7674=Mrk533	2	SBbc-M	$3.796 \pm 0.561$	–	24

**Table A1.** Morphological information for the host galaxies of the extended 12  $\mu\text{m}$  Seyfert sample.

by an asterisk symbol (\*); *Column 6*: Peak NVSS flux density determined from a Gaussian fit (mJy/beam). NVSS flux density upper-limits of  $5\text{-}\sigma$  have been assumed for 5 sources for which no NVSS counterpart was found within the search radius ( $1\text{-}\sigma = 0.45$  mJy/beam); *Column 7*: Integrated NVSS flux density (mJy/beam).

Galaxy	Type	RA(J2000) (h m s)	Dec(J2000) ( $^{\circ}$ ' ")	$\theta_{\text{sep}}$ (")	SNVSS peak (mJy/B)	SNVSS integ. (mJy/B)
Mrk 335	1	00 06 19.45	+20 12 10.3	1.4	7.6	7.6
NGC 34=Mrk 938	s	00 11 06.54	-12 06 27.4	0.4	62.4	67.8
NGC 262=Mrk 348	2	00 48 47.15	+31 57 25.3	0.3	292.7	292.7
IZW1	1	00 53 34.77	+12 41 33.8	3.3	8.8	8.8
E541-IG12	2	01 02 17.91	-19 40 06.5	7.7	4.8	4.8
NGC 424=TOL0109	2	01 11 27.71	-38 04 59.6	1.3	23.3	23.3
NGC 526A	1	01 23 54.57	-35 03 57.5	2.9	11.5	13.9
NGC 513	2	01 24 26.66	+33 47 55.8	3.0	48.4	53.8
F01475-0740	2	01 50 02.66	-07 25 49.2	0.8	318.8	318.8
Mrk 1034	1	02 23 21.71	+32 11 47.0	3.7	42.3	51.6
MCG-3-7-11	1	02 24 40.45	-19 08 31.7	1.8	28.2	31.3
NGC 931=Mrk 1040	1	02 25 16.46	+31 05 19.9	*7.1	9.3	15.5
NGC 1056=Mrk 1183	2	02 42 48.28	+28 34 28.1	3.6	27.8	38.6
NGC 1068	2	02 42 40.72	-00 00 47.7	4.2	4468.5	4857.1
NGC 1097	L	02 46 18.93	-30 16 29.3	0.9	200.6	250.7
NGC 1125	2	02 51 40.44	-16 39 02.1	0.2	54.8	58.3
NGC 1143/4	2	02 55 12.16	-00 10 58.7	2.3	140.1	155.7
MCG-2-8-39	2	02 58 06.76	-11 36 50.2	*7.5	9.0	9.0
NGC 1194	2	03 03 49.67	-01 06 17.3	9.1	2.9	2.9
NGC 1320=Mrk 607	2	03 24 48.81	-03 02 29.5	3.5	6.5	6.5
NGC 1365	1	03 33 36.46	-36 08 25.9	5.6	331.1	376.2
NGC 1386	s	03 36 46.22	-35 59 57.3	0.3	35.1	37.7
F03362-1642	2	03 38 33.58	-16 32 15.6	2.8	9.3	9.3
F03450+0055	1	03 47 40.17	+01 05 14.6	0.7	32.5	32.5
Mrk 618	1	04 36 22.34	-10 22 32.7	1.4	17.3	17.3
F04385-0828	2	04 40 54.33	-08 22 20.7	9.5	11.7	18.9
NGC 1667	2	04 48 37.06	-06 19 13.0	1.9	56.9	76.9
MCG-5-13-17	1	05 19 35.72	-32 39 29.5	1.5	12.7	14.9
F05189-2524	2	05 21 01.38	-25 21 45.0	0.4	29.1	29.1
F05563-3820	1	05 58 02.20	-38 20 02.4	5.9	34.9	34.9
Mrk 6	2	06 52 12.47	+74 25 37.0	0.6	259.7	276.3
Mrk 9	1	07 36 56.17	+58 46 16.9	7.4	4.1	4.1
Mrk 79	1	07 42 32.84	+49 48 34.1	0.8	18.3	22.3
F07599+6508	1	08 04 30.75	+64 59 53.5	1.9	39.7	39.7
NGC 2639	1	08 43 38.16	+50 12 20.4	0.9	109.0	116.0
F08572+3915	2	09 00 25.58	+39 03 52.8	2.7	4.7	4.7
Mrk 704	1	09 18 26.05	+16 18 21.2	1.7	6.6	6.6
UGC 5101	1	09 35 51.83	+61 21 12.9	2.0	145.1	170.7
NGC 2992	2	09 45 42.00	-14 19 34.6	0.8	226.6	226.6
Mrk 1239	1	09 52 19.11	-01 36 43.5	0.2	62.8	62.8
NGC 3031=M 81	L	09 55 33.28	+69 03 55.0	0.6	82.4	88.6
NGC 3079	2	10 01 57.82	+55 40 48.5	1.2	491.9	768.6
NGC 3227	1	10 23 30.55	+19 51 54.8	0.7	86.2	100.2
NGC 3511	1	11 00 57.39	-22 49 03.9	*1.5	15.4	77.0
NGC 3516	1	11 06 47.71	+72 34 10.3	3.2	27.6	32.5
M+0-29-23	2	11 18 38.95	-02 42 34.7	*18.3	35.3	35.3
NGC 3660	2	11 21 00.18	-08 22 56.1	*12.6	5.7	14.6
NGC 3982	2	11 56 27.95	+55 07 30.9	1.6	37.9	57.4
NGC 4051	1	12 03 09.28	+44 31 54.0	3.7	19.6	98.0
NGC 4151	1	12 10 32.52	+39 24 20.9	1.1	360.1	360.1
Mrk 766	1	12 18 26.43	+29 48 47.3	1.3	37.0	39.8
NGC 4388	2	12 25 46.97	+12 39 43.7	3.8	94.5	121.2
NGC 4579	1	12 37 43.74	+11 49 08.0	4.2	58.0	98.3
NGC 4593	1	12 39 39.31	-05 20 35.9	3.7	4.8	4.8
NGC 4594	1	12 39 59.40	-11 37 23.5	0.6	85.0	94.4
NGC 4602	1	12 38 02.13	-04 51 25.3	*18.0	16.3	40.8
TOL1238-364	2	12 40 52.85	-36 45 20.1	1.0	73.6	88.7
MCG-2-33-34	1	12 52 12.65	-13 24 52.8	2.6	14.3	14.3
Mrk 231=UGC 8058	1	12 56 14.13	+56 52 23.8	1.7	271.9	309.0
NGC 4922A/B	2	13 01 25.23	+29 18 50.3	0.8	39.3	39.3
NGC 4941	2	13 04 13.02	-05 33 03.5	2.5	16.8	20.2
NGC 4968	2	13 07 06.00	-23 40 36.1	1.4	34.9	34.9
NGC 5005	2	13 10 56.16	+37 03 32.3	1.3	86.9	181.0
NGC 5033	1	13 13 27.28	+36 35 40.4	3.4	82.2	122.7
MCG-3-34-63	2	13 22 24.58	-16 43 43.1	1.8	275.3	275.3
NGC 5135	2	13 22 56.51	-29 34 25.6	*14.8	187.2	201.3
NGC 5194=M 51	2	13 29 52.65	+47 11 45.7	2.9	103.6	431.7
F13349+2438	1	13 37 18.73	+24 23 02.8	0.6	20.0	20.0
NGC 5256=Mrk 266	2	13 38 17.60	+48 16 38.4	6.6	114.1	129.7
Mrk 273=UGC 8696	2	13 44 42.21	+55 53 13.1	0.8	134.9	145.1
I4329A	1	13 49 19.23	-30 18 33.7	0.6	66.8	66.8
NGC 5347	2	13 53 18.04	+33 29 25.6	3.2	6.0	6.0
Mrk 463	2	13 56 02.86	+18 22 19.0	0.5	381.0	381.0
NGC 5506	2	14 13 14.84	-03 12 27.0	0.9	339.4	339.4
NGC 5548	1	14 17 59.32	+25 08 13.5	3.0	24.7	29.1
Mrk 817	1	14 36 22.07	+58 47 41.6	2.2	11.7	11.7
F15091-2107	1	15 11 59.82	-21 19 00.1	1.5	47.3	47.3
NGC 5929	2	15 26 06.69	+41 40 21.0	9.5	85.8	110.0
NGC 5953	2	15 34 32.70	+15 11 40.9	5.7	68.4	91.2
UGC 9913=ARP220	s	15 34 57.26	+23 30 11.1	1.0	326.8	326.8
MCG-2-40-4	2	15 48 24.90	-13 45 28.5	1.6	26.1	30.7
F15480-0344	2	15 50 41.47	-03 53 17.1	1.1	42.2	42.2
Mrk 509	1	20 44 09.68	-10 43 23.0	2.0	16.4	19.3
UGC 11680=Mrk 897	2	21 07 45.86	+03 52 40.5	0.1	17.3	17.3
NGC 7130=15135	2	21 48 19.57	-34 57 04.8	0.6	169.3	190.2
NGC 7172	2	22 02 01.96	-31 52 10.5	0.9	33.8	37.6
F22017+0319	2	22 04 19.64	+03 33 48.7	8.2	12.1	18.3
NGC 7314	1	22 35 46.43	-26 03 01.7	5.4	7.7	33.5
MCG-3-58-7	2	22 49 37.08	-19 16 25.5	2.3	12.7	12.7
NGC 7469	1	23 03 15.61	+08 52 26.3	0.2	181.0	181.0
NGC 7603=Mrk 530	1	23 18 56.68	+00 14 37.2	0.9	24.9	24.9
NGC 7674=Mrk 533	2	23 27 56.69	+08 46 43.3	1.0	221.4	221.4
NGC 1241	2	—	—	>10	2.3	2.3
CGCG381-051	2	—	—	>10	2.3	2.3
UGC 7064	1	—	—	*>20	2.3	2.3
NGC 4501	2	—	—	*>20	2.3	2.3
MCG-6-30-15	1	—	—	*>20	2.3	2.3

Table A2. The NVSS counterparts of Seyferts from the extended 12  $\mu\text{m}$  sample.

Scaling Factor	P(null hypothesis)				
	Gehan's (perm.)	Gehan's (hyper.)	Logrank	Peto & Peto	Peto & Prentice
1/8	0.19%	0.20%	0.60%	0.20%	0.18%
1/6	0.91%	0.94%	2.54%	0.92%	0.90%
1/4	4.45%	4.59%	7.84%	4.38%	4.40%
1/2	36.94%	37.25%	37.56%	36.20%	36.61%
1	70.86%	70.87%	77.76%	71.22%	71.48%
2	13.96%	13.60%	26.09%	14.43%	14.35%
4	0.85%	0.70%	4.14%	0.91%	0.83%
6	0.09%	0.06%	0.51%	0.09%	0.07%
8	0.03%	0.01%	0.21%	0.03%	0.02%

**Table B1.** The probability of the null hypothesis that type 1 and type 2 Seyferts have 8.4 GHz A-configuration luminosities drawn at random from the same parent population varies as scaling factors of one-eighth to eight are applied to the type 1 sub-population. The luminosity of each type 1 Seyfert was multiplied by the scaling factor and the probability of the null hypothesis was re-calculated. The probability of the null hypothesis is less than 5% for all statistical tests with scaling factors less than or equal to one sixth, or greater than or equal to four.

Scaling Factor	P(null hypothesis)				
	Gehan's (perm.)	Gehan's (hyper.)	Logrank	Peto & Peto	Peto & Prentice
1/10	0.07%	0.06%	0.27%	0.16%	0.02%
1/8	0.12%	0.11%	0.68%	0.29%	0.17%
1/6	0.35%	0.34%	1.86%	0.74%	0.46%
1/4	1.34%	1.34%	6.17%	2.51%	2.17%
1/2	11.37%	11.53%	29.06%	16.82%	16.20%
1	53.00%	53.16%	78.93%	59.69%	59.51%
2	89.34%	89.31%	82.46%	87.00%	86.97%
4	23.53%	22.71%	32.29%	24.82%	23.77%
6	8.65%	7.78%	16.82%	10.54%	9.32%
8	3.07%	2.45%	7.88%	4.26%	3.28%
10	1.42%	1.00%	3.95%	2.19%	1.46%

**Table B2.** The probability of the null hypothesis, that type 1 and type 2 Seyferts have 8.4 GHz A-configuration sizes drawn at random from the same parent population, varies as scaling factors of one tenth to ten are applied to the type 1 sub-population. The size of each type 1 Seyfert was multiplied by the scaling factor and the probability of the null hypothesis was re-calculated. The probability of the null hypothesis is less than 5% for all statistical tests with scaling factors less than or equal to one sixth and greater than or equal to 10.

## APPENDIX B: STATISTICAL TEST RESULTS

We have estimated the power of a statistical test to reject a null hypothesis by making trials with the observational data (see Section 3).

Table B1 shows the results of scaling the 8.4 GHz A-configuration luminosity of the Seyfert 1 sub-population and repeating two-sample tests.

Table B2 shows the results of scaling the radio sizes of the Seyfert 1 sub-population and repeating two-sample tests.

## APPENDIX C: SPACE DENSITIES OF THE EXTENDED 12-MICRON SEYFERTS

The differential radio luminosity function shown in Figure 2 has been estimated using a method based on the  $V/V_{\max}$  method described by Huchra & Sargent (1973). The density of sources per luminosity interval,  $\Phi(L)$  is given by,

$$\Phi(L) = \frac{4\pi}{\Omega f \Delta L} \sum_{i=1}^n \frac{1}{V_{\max}(L)} \quad (\text{Mpc}^{-3} \text{mag}^{-1}), \quad (\text{C1})$$

where  $\Omega$  is the solid angle covered by the sample (7.26 steradians),  $f$  is the fraction of the sample for which radio observations were obtained (38/47 for Seyfert 1s and 48/60 for Seyfert 2s),  $\Delta L = 10^{0.4} \text{ WHz}^{-1}$  is the bin width and  $V_{\max}(L)$  is the maximum accessible volume for each source and is chosen as the lower of the two values defined by the radio and 12  $\mu\text{m}$  flux densities and flux limits. Individual values of  $\Phi(L)$  are given in Table C.

No luminosity upper-limits have been used to construct the differential radio luminosity function and therefore  $\Phi(L)$  is likely to be under-estimated at low luminosities. However, the Kaplan-Meier estimator cannot be used to estimate the shape of the differential luminosity function accurately because it is not strictly defined when the distribution of censored data points is not random; the radio luminosity upper-limits we have obtained for 12 sources are grouped towards the lower luminosity end of the radio luminosity distribution and there is an extremely low probability that they were drawn at random from the sample ( $2 \times 10^{-05}\%$  according to the KS test). Note that non-random censorship does not invalidate two-sample tests for which accurate estimates of the true distribution functions are not required. The true value of  $\Phi(L)$  at low luminosities could be at least a factor of four higher than that given in Table C; the Kaplan-Meier estimator indicates that approximately 4 undetected type 1 sources could be found in the luminosity bin centered at  $10 \times 10^{18.8} \text{ WHz}^{-1}$ , their effect on  $\Phi(L)$  depends on the values of  $V_{\max}$  which are likely to be defined by their 12  $\mu\text{m}$  flux densities.

Assigning errors to  $\Phi(L)$  is not straightforward; in the majority of cases  $V_{\max}(L)$  values are determined by *IRAS* 12  $\mu\text{m}$  fluxes which may be dependent on 8.4 GHz VLA A-configuration fluxes. For simplicity, one-sigma fractional uncertainties on  $\Phi(L)$  are taken as  $1/\sqrt{N}$ , where  $N$  is the number of sources in each luminosity bin.

## APPENDIX D: THE RADIO-INFRARED LUMINOSITY-LUMINOSITY PLANE.

In Section 4.1 we showed that evidence of a correlation between 8.4 GHz A-configuration luminosities and *IRAS* 12  $\mu\text{m}$  luminosities is weak when observational limitations are taken into account. Here we describe the derivation of the limits defined by the Malmquist bias and the flux limits which are shown in Figure 6.

The upper-left portion of Figure 6 is under-populated because of the Malmquist bias; sources with low 12  $\mu\text{m}$  luminosities are only selected from a relatively nearby volume of space in which there is a low probability of finding sources with high radio luminosities (which are intrinsically rare). The dashed line in Figure 6 represents the limit above which

log(L <sub>rad</sub> ) (bin cent.)	All Seyferts			Seyfert 1s			Seyfert 2s		
	N	logΦ	ΔlogΦ	N	logΦ	ΔlogΦ	N	logΦ	ΔlogΦ
18.8	2	-4.07	0.23	1	-4.41	0.30	1	-4.35	0.30
19.2	—	—	—	—	—	—	—	—	—
19.6	3	-4.52	0.20	1	-5.12	0.30	2	-4.65	0.23
20.0	5	-4.29	0.16	2	-4.72	0.23	3	-4.49	0.20
20.4	7	-4.70	0.14	2	-5.11	0.23	5	-4.91	0.16
20.8	8	-4.97	0.13	4	-5.44	0.18	4	-5.15	0.18
21.2	11	-4.73	0.11	5	-4.82	0.16	6	-5.48	0.15
21.6	19	-5.14	0.09	9	-5.80	0.12	10	-5.24	0.12
22.0	8	-5.44	0.13	6	-5.48	0.15	2	-6.53	0.23
22.4	12	-5.50	0.11	2	-5.64	0.23	10	-6.05	0.12
22.8	6	-6.33	0.15	3	-7.41	0.20	3	-6.36	0.20
23.2	4	-6.51	0.18	2	-7.60	0.23	2	-6.54	0.23
23.6	—	—	—	—	—	—	—	—	—
24.0	1	-7.84	0.30	1	-7.84	0.30	—	—	—

**Table C1.** The space densities of the extended 12 μm Seyferts at 8.4 GHz.

there is less than a 4.6% probability of finding a Seyfert and has been estimated using the following relationship;

$$P(L_{\text{rad}}|L_{\text{IR}}) = \Phi_{\text{rad}} \cdot \frac{1}{\Phi_{\text{IR}}} = 4.6\%, \quad (\text{D1})$$

where  $P(L_{\text{rad}}|L_{\text{IR}})$  is the probability of finding a source with a radio luminosity,  $L_{\text{rad}}$ , given that it has an infrared luminosity  $L_{\text{IR}}$ ,  $\Phi_{\text{rad}}$  is the space density of Seyferts per radio magnitude and  $\Phi_{\text{IR}}$  is the space density of Seyferts per infrared magnitude ( $1/\Phi_{\text{IR}}$  is the characteristic volume sampled in a given infrared luminosity interval). The values of  $L_{\text{rad}}$  and  $L_{\text{IR}}$  which correspond to  $\Phi_{\text{rad}}$  and  $\Phi_{\text{IR}}$  have been estimated from the differential 12 μm luminosity function (Rush, Malkan & Spinoglio 1993) and the differential 8.4 GHz luminosity function (Fig. 2c).

The lower-right portion of Figure 6 is under-populated because of a combination of the infrared and radio flux limits; a given infrared luminosity defines a maximum distance at which a source may be detected above the infrared flux limit and the radio detection threshold defines the minimum detectable radio luminosity for sources at that distance. The dotted line in Figure 6 shows the minimum detectable radio luminosity at the maximum distance allowed by a given infrared luminosity assuming an infrared flux limit of 0.22 Jy and radio detection threshold of 162 μJy; distant sources are unlikely to be found below this limit. Note that the radio detection threshold varied from source to source according to the map quality.

#### APPENDIX E: NEWLY-IDENTIFIED SEYFERTS IN THE EXTENDED 12-MICRON SAMPLE.

Table E1 shows 38 sources which were classified as ‘normal galaxies’ or ‘high-far-infrared’ galaxies by Rush et al. but which are classified as Seyferts in the NED. Since NED classifications are not always reliable, an accurate re-definition of the sample will require careful inspection of individual spectra; where we are aware of them, we have provided references to alternative classifications. Table E1 is arranged as follows; *Column 1*: Galaxy name; *Column 2*: NED Seyfert type; *Column 3*: Alternative galaxy type as taken from the following sources: (1) Veron, Goncalves & Veron-Cetty (1997) (2) Kinney et al. (1993) (3) Lancon,

Rocca-Volmerange & Thuan (1996) (4) Forbes, Boisson & Ward (1992) (5) Kinney et al. (1984) (6) Calzetti, Kinney & Storchi-Bergmann (1994) (7) Taniguchi et al. (1999) (8) Goncalves, Veron-Cetty & Veron (1999).

Another AGN from the extended 12 μm sample which was classified as a ‘normal galaxy’ by Rush et al. is the exceptional source NGC 5232. The optical spectrum of this source is similar to a normal, early-type galaxy (Drinkwater et al. 1997), but it has a higher NVSS to *IRAS* flux ratio (0.56) than all 92 extended 12 μm Seyferts for which NVSS data is available. This source is possibly one of the few examples of a spiral radio galaxy; the NVSS map appears to show a hundred-kiloparsec-scale jet which straddles the nucleus of a SA(rs)0/a host galaxy (Condon, Anderson & Broderick 1995).

#### REFERENCES

- Akritas M. G., Siebert J., 1996, MNRAS, 278, 919
- Antonucci R., 1993, ARA&A, 31, 473
- Axon D. J., Marconi A., Capetti A., Maccetto F. D., Schreier E., Robinson A., 1998, ApJ, 496, L75
- Barcons X., Franceschini A., De Zotti G., Danese L., Miyaji T., 1995, ApJ, 455, 480
- Baum S. A., O’Dea C. P., Dallacasa D., de Bruyn A., Pedlar A., 1993, ApJ, 419, 553
- Bicay M. D., Helou G., 1990, ApJ, 362, 59
- Calzetti D., Kinney A. L., Storchi-Bergmann T., 1994, ApJ, 429, 582
- Capetti A., Axon D. J., Macchetto F. D., Marconi A., Winge C., 1999, ApJ, 516, 187
- Christopoulou P. E., Holloway A. J., Steffen W., Mundell C. G., Thean A. H. C., Goudis C. D., Meaburn J., Pedlar A., 1997, MNRAS, 284, 385
- Colbert E. J. M., Baum S. A., Gallimore J. F., O’Dea C. P., Christensen J. A., 1996, ApJ, 467, 551



Galaxy	Type (NED)	Type (other)
MCG-4-2-18	1.8	
NGC 613	Sy	Composite (1)
M+0-7-41	2	
NGC 1433	2	HII (2)
MCG-5-11-6	2	
F04259-0440	2	
NGC 1614	2	HII (3)
NGC 1672	2	Transition (1)
NGC 1808	2	HII (4)
NGC 2655	2	
NGC 2782	1	HII (5)
NGC 3094	2	
NGC 3147	2	
NGC 3367	Sy	
NGC 3486	2	
NGC 3593	2	
NGC 3735	2	
NGC 3822	2	
NGC 3976	2	
NGC 4699	Sy	
NGC 4725	Sy	
NGC 4995	Sy	
Markarian 1361	2	
NGC 5899	2	
NGC 5905	1	Transition (1)
CGCG 022-021	1.9	
UGC 9944	2	
NGC 6217	2	HII (6)
NGC 6240	2	
NGC 6552	2	
IC 5169	2	
ESO 344-G16	1.5	
ESO 148-IG02	2	HII (7)
IC 5298	2	HII (8)
NGC 7678	2	
NGC 7733/4	2	
MCG+2-60-17	2	
Markarian 331	2	HII (3)

**Table E1.** Sources classified as galaxies or high-infrared galaxies by Rush et al. (1993) which are classified as Seyferts in the NED.

Colbert E. J. M., Baum S. A., O’Dea C. P., Veilleux S., 1998, ApJ, 496, 786

Condon J. J., Broderick J. J., 1986, AJ, 92, 94

Condon J. J., Broderick J. J., 1988, AJ, 96, 30

Condon J. J., Anderson E., Broderick J. J., 1995, AJ, 109, 2318

Condon J. J., Cotton W. D., Greisen E. W., Yin Q. F., Perley R. A., Taylor G. B., Broderick J. J., 1998, AJ, 115, 1693

de Bruyn A. G., Wilson A. S., 1978, A&A, 64, 433

de Jong T., Klein U., Wielebinski R., Wunderlich E., 1985, A&A, 147, L6

de Vaucouleurs G., de Vaucouleurs A., Corwin J. R., Buta R. J., Paturel G., Fouque P., 1991, in Third reference catalogue of bright galaxies, version 9 (1991). p. 0

Dopita M. A., Heisler C., Lumsden S., Bailey J., 1998, ApJ, 498, 570

Drinkwater M. J. et al., 1997, MNRAS, 284, 85

Edelson R. A., 1987, ApJ, 313, 651

Efstathiou A., Rowan-Robinson M., 1995, MNRAS, 273, 649

Elmoultie M., Haynes R. F., Jones K. L., Sadler E. M., Ehle M., 1998, MNRAS, 297, 1202

Fadda D., Giuricin G., Granato G. L., Vecchies D., 1998, ApJ, 496, 117

Falcke H., Wilson A. S., Simpson C., 1998, ApJ, 502, 199

Feigelson E. D., Nelson P., 1985, ApJ, 293, 192

Forbes D. A., Boisson C., Ward M. J., 1992, MNRAS, 259, 293

Franceschini A., Vercellone S., Fabian A. C., 1998, MNRAS, 297, 817

Giuricin G., Mardirossian F., Mezzetti M., Bertotti G., 1990, ApJS, 72, 551

Goncalves A. C., Veron-Cetty M. P., Veron P., 1999, A&AS, 135, 437

Granato G., Danese L., 1994, MNRAS, 268, 235

Heckman T., 1995, ApJ, 446, 101

Heisler C., Lumsden S., Bailey J., 1997, Nature, 385, 700

Helou G., Madore B., Schmitz M., Wu X., Corwin H., LaGue Jr. C. Bennett J., Sun H. in Egret D., Albrecht M. A., eds, Information and On-Line Data in Astronomy, p. 95, Kluwer, Dordrecht, 1995

Helou G., Soifer B. T., Rowan-Robinson M., 1985, ApJ, 298, L7

Hewitt A., Burbidge G., 1991, ApJS, 75, 297

Ho L. C., 1999, ApJ, 510, 631

Huchra J., Burg R., 1992, ApJ, 393, 90

Huchra J. P., Sargent W. L. W., 1973, ApJ, 186, 433

Hunt L. K., Malkan M. A., 1999, ApJ, 516, 660

Isobe T., Feigelson E. D., Nelson P., 1986, ApJ, 306, 490

Kay L. E., Moran E. C., 1998, PASP, 110, 1003

Kinney A. L., Bregman J. N., Huggins P. J., Glassgold A. E., Cohen R. D., 1984, PASP, 96, 398

Kinney A. L., Bohlin R. C., Calzetti D., Panagia N., Wyse R. F. G., 1993, ApJS, 86, 5

Kormendy J., Richstone D., 1995, ARA&A, 33, 581

Krolik J., Lepp S., 1989, ApJ, 347, 179

Kukula M. J., Pedlar A., Baum S. A., O’Dea C. P., 1995, MNRAS, 276, 1262

- Lancon A., Rocca-Volmerange B., Thuan T. X., 1996, *A&A*, 115, 253
- Lavalley M., Isobe T., Feigelson E., 1992, *ASP Conf. Ser. 25: Astronomical Data Analysis Software and Systems I*, 1, 245
- Magorrian J. et al., 1998, *AJ*, 115, 2285
- Maiolino R., Ruiz M., Rieke G. H., Keller L., 1995, *ApJ*, 446, 561
- Malkan M., Gorjian V., Tam R., 1998, *ApJS*, 117, 25
- Miyoshi M., Moran J., Herrnstein J., Greenhill L., 1995, *Nature*, 373, 127
- Moles M., Marquez I., Perez E., 1995, *ApJ*, 438, 604
- Moran E. C., Halpern J. P., Bothun G. D., Becker R. H., 1992, *AJ*, 104, 990
- Morganti R., Tsvetanov Z., Gallimore J., Allen M., 1999, *A&AS*, 137, 457
- Moshir M. et al. Explanatory Supplement to the IRAS Faint Source Survey, Version 2. 1991, (Pasadena:JPL)
- Mulchaey J. S., Wilson A. S., Tsvetanov Z., 1996a, *ApJS*, 102, 309
- Mulchaey J. S., Wilson A. S., Tsvetanov Z., 1996b, *ApJ*, 467, 197
- Nagar N. M., Wilson A. S., 1999, *ApJ*, 516, 97
- Nagar N. M., Wilson A. S., Mulchaey J. S., Gallimore J. F., 1999, *ApJS*, 120, 209
- Neff S., de Bruyn A., 1983, *A&A*, 128, 318
- Niklas S., 1997, *A&A*, 322, 29
- O'Dea C. P., 1998, *PASP*, 110, 493
- Paturel G. et al., 1996, *A&AS*, 124, 109
- Pedlar A., Meaburn J., Axon D., Unger S. Whittle D., Meurs J., Guerrine N., Ward M., 1989, *MNRAS*, 238, 863
- Pier E., Krolik J., 1992, *ApJ*, 401, 99
- Rodriguez Espinosa J. M., Rudy R. J., Jones B., 1987, *ApJ*, 312, 555
- Roy A., Norris R. P., Kesteven M. J., Troup E. R., Reynolds J. E., 1994, *ApJ*, 432, 496
- Roy A., Norris R. P., Kesteven M. J., Troup E. R., Reynolds J. E., 1998, *MNRAS*, 301, 1019
- Rush B., Malkan M. A., Edelson R., 1996, *ApJ*, 473, 130
- Rush B., Malkan M. A., Spinoglio L., 1993, *ApJS*, 89, 1
- Sadler E. M., Jenkins C. R., Kotanyi C. G., 1989, *MNRAS*, 240, 591
- Salzer J., 1989, *ApJ*, 347, 152
- Sanders D. B., Soifer B. T., Elias J. H., Madore B. F., Matthews K., Neugebauer G., Scoville N. Z., 1988, *ApJ*, 325, 74
- Schmitt H. R., Kinney A. L., Storchi-Bergmann T., Antonucci R., 1997, *ApJ*, 477, 623
- Schommer R. A., Caldwell N., Wilson A. S., Baldwin J. A., Phillips M. M., Williams T. B., Turtle A. J., 1988, *ApJ*, 324, 154
- Schulz H., 1988, *A&A*, 203, 233
- Smith H., Lonsdale C., Lonsdale C., Diamond P., 1998, *ApJ*, 493, L17
- Spinoglio L., Malkan M. A., 1989, *ApJ*, 342, 83
- Taniguchi Y., Yoshino A., Ohyama Y., Nishiura S., 1999, *ApJ*, 514, 660
- Terlevich R., Guillermo T.-T., Franco J., Melnick J., 1992, *MNRAS*, 255, 713
- Thean A., Pedlar A., Kukula M., Baum S. A., O'Dea C. P. 2000a. *MNRAS*, in press astro-ph/0001459
- Thean A., Pedlar A., Kukula M., Baum S. A., O'Dea C. P. 2000b. in van Haarlem M. P., eds, *Perspectives in Radio Astronomy: Science with Large Antenna Arrays*, in press
- Ulvestad J. S., Wilson A. S., 1984a, *ApJ*, 278, 544
- Ulvestad J. S., Wilson A. S., 1984b, *ApJ*, 285, 439
- Ulvestad J. S., Wilson A. S., 1989, *ApJ*, 343, 659
- Ulvestad J. S., Wrobel J. M., Roy A. L., Wilson A. S., Falcke H., Krichbaum T. P., 1999, *ApJ*, 517, L81
- Unger S. W., Pedlar A., Neff S. G., de Bruyn A. G., 1984, *MNRAS*, 209, 15
- Veron-Cetty M. P., Veron P., 1991, *ESO Sci. Rep.*, 10
- Veron P., Goncalves A. C., Veron-Cetty M. P., 1997, *A&A*, 319, 52
- Whittle M., 1992, *ApJ*, 387, 121
- Wilson A. S., Tsvetanov Z., 1994, *AJ*, 107, 1227
- Wilson A. S., Braatz J. A., Heckman T. M., Krolik J. H., Miley G. K., 1993, *ApJ*, 419, L61
- Wilson A. S., 1988, *A&A*, 206, 41
- Wilson A. S. in Duric N., Crane P. C., eds, *NRAO Workshop on the Interpretation of Modern Synthesis Observations of Spiral Galaxies.*, p. 277, *Astron. Soc. Pac.*, 1991